

# Ammonia–water ice laboratory studies relevant to outer Solar System surfaces

M.H. Moore<sup>a,\*</sup>, R.F. Ferrante<sup>b</sup>, R.L. Hudson<sup>c</sup>, J.N. Stone<sup>b</sup>

<sup>a</sup> Code 691, Astrochemistry Branch, NASA Goddard Space Flight Center, Greenbelt, MD 20771, USA

<sup>b</sup> Department of Chemistry, US Naval Academy, Annapolis, MD 21402, USA

<sup>c</sup> Department of Chemistry, Eckerd College, St. Petersburg, FL 33733, USA

Received 14 November 2006; revised 26 January 2007

Available online 30 March 2007

## Abstract

Although water- and ammonia-ices have been observed or postulated as important components of the icy surfaces of planetary satellites in the outer Solar System, significant gaps exist in our knowledge of the spectra and behavior of such mixtures under astrophysical conditions. To that end, we have completed low-temperature spectroscopic studies (1–20  $\mu\text{m}$ ) of water–ammonia mixtures, with an emphasis on features in the near-IR, a region which is accessible to ground-based observations. The influences of composition, formation temperature, thermal- and radiation-processing, and phase (crystalline or amorphous) of the components were examined. Spectra of both pure  $\text{NH}_3$  and  $\text{H}_2\text{O}$ – $\text{NH}_3$  icy mixtures with ratios from 0.7 to 57 were measured at temperatures from 10 to 120 K. Conditions for the formation and thermal stability of the ammonia hemihydrate ( $2\text{NH}_3\cdot\text{H}_2\text{O}$ ) and the ammonia monohydrate ( $\text{NH}_3\cdot\text{H}_2\text{O}$ ) have been examined. Band positions of  $\text{NH}_3$  in different  $\text{H}_2\text{O}$ -ices and major band positions of the hydrates were measured. We report spectral shifts that depend on concentration and temperature. The radiation-induced amorphization of the hemihydrate was observed and the radiation destruction of  $\text{NH}_3$  in  $\text{H}_2\text{O}$ -ices was measured. Implications of these results for the formation, stability, and detection of ammonia on outer satellite surfaces are discussed.

© 2007 Elsevier Inc. All rights reserved.

**Keywords:** Ices; Charon; Trans-neptunian objects; Satellites, surfaces; Spectroscopy

## 1. Introduction

A near-IR absorption feature near 2.2  $\mu\text{m}$ , attributed to  $\text{NH}_3$ , has been observed in the spectra of Charon (Brown and Calvin, 2000; Dumas et al., 2001; Cook et al., 2006, 2007, Quaoar (Jewitt and Luu, 2004), and Miranda (Bauer et al., 2002). An equally intense  $\text{NH}_3$  band at 2.0  $\mu\text{m}$  has not been detected, presumably because it is blended with the 2.0- $\mu\text{m}$  band of  $\text{H}_2\text{O}$ , the dominant icy material on these objects. The latest observations of Charon (Cook et al., 2007) find hemispheric dichotomies in ice composition. Sub-Pluto and anti-Pluto spectra are best fit to minima located at 2.1995 and 2.2131  $\mu\text{m}$ , respectively, using models that include ammonia hydrates. Models using  $\text{NH}_3$  hydrate spectra are thought to be consistent with the idea that liquid water–ammonia cryomagma with specific  $\text{H}_2\text{O}$  and  $\text{NH}_3$

concentrations (e.g., the ammonia dihydrate,  $\text{NH}_3\cdot 2\text{H}_2\text{O}$ ) periodically spills over the surface and cools, losing  $\text{NH}_3$  preferentially. This process would result in crystalline-phase  $\text{H}_2\text{O}$ -ice, which is consistent with the 1.65- $\mu\text{m}$  signature of that material observed on Charon. The Quaoar  $\text{NH}_3$  band is centered at  $2.22 \pm 0.005 \mu\text{m}$ , and a model fit results in a 3%  $\text{NH}_3\cdot\text{H}_2\text{O}$  abundance. On Miranda the weak band near 2.2  $\mu\text{m}$  was best modeled by including 3% mass fraction of  $\text{NH}_3\cdot\text{H}_2\text{O}$ , but the fit was not unique. These observations, along with mounting evidence for  $\text{NH}_3$  ice on Enceladus (Emery et al., 2005; Verbiscer et al., 2006), are not surprising since  $\text{NH}_3$  is predicted to be one of the more abundant species incorporated into outer Solar System bodies (Lewis, 1972).

There are three known stoichiometric water–ammonia solids termed ammonia hydrates: the dihydrate  $\text{NH}_3\cdot 2\text{H}_2\text{O}$ , the monohydrate  $\text{NH}_3\cdot\text{H}_2\text{O}$ , and the hemihydrate  $2\text{NH}_3\cdot\text{H}_2\text{O}$  with compositions of 32, 49, and 65 mass percent ammonia, respectively. As ices, these hydrates are crystalline materials with

\* Corresponding author. Fax: +1 301 286 0440.

E-mail address: [marla.h.moore@nasa.gov](mailto:marla.h.moore@nasa.gov) (M.H. Moore).

Table 1  
Estimated particle radiation doses for selected icy Solar System objects

Object	Ices detected	Distance (AU)	Particle radiation environment	Dose at indicated depth (eV 16-amu-molecule <sup>-1</sup> ) <sup>a</sup>		
				1-m	100- $\mu$ m	1- $\mu$ m
Saturn's moon Enceladus	H <sub>2</sub> O, NH <sub>3</sub> ?	9.6	O <sup>+</sup> and electrons in magnetosphere of Saturn <sup>b</sup>	100/>10 <sup>5</sup> yrs	100/6 × 10 <sup>3</sup> yrs	100/10 <sup>4</sup> yrs
Uranus' moon Miranda	H <sub>2</sub> O, NH <sub>3</sub> (NH <sub>3</sub> hydrate?)	19.2	Proton and electrons in magnetosphere of Uranus <sup>c</sup>	1000's/10 <sup>4</sup> –10 <sup>6</sup> yrs	1000's/10 <sup>4</sup> –10 <sup>6</sup> yrs	1000's/10 <sup>4</sup> –10 <sup>6</sup> yrs
Pluto's moon Charon	H <sub>2</sub> O, NH <sub>3</sub> , NH <sub>3</sub> hydrate	40	SEP, ACR and GCR ions <sup>d</sup>	10's	10's	10's
KBO Quaoar	H <sub>2</sub> O, NH <sub>3</sub> , NH <sub>3</sub> hydrate?	<48–~1000	SEP, ACR and GCR ions <sup>d</sup>	10's	10's–1000's	10's–10,000's
Oort cloud comets	Gases <sup>e</sup> : H <sub>2</sub> O, CO, CO <sub>2</sub> , CH <sub>3</sub> OH, CH <sub>4</sub> , H <sub>2</sub> CO, NH <sub>3</sub> , OCS, HCOOH, HCN, C <sub>2</sub> H <sub>6</sub> , C <sub>2</sub> H <sub>2</sub>	>10 <sup>4</sup>	SEP, ACR and GCR ions <sup>d</sup>	10's	1000's	10,000's

<sup>a</sup> Assumes an ice density of 1.0 g cm<sup>-3</sup>.

<sup>b</sup> Calculations assume Enceladus' doses are similar to those calculated for Dione. See Sittler et al. (2006).

<sup>c</sup> Rough estimates based on Krimigis et al. (1986).

<sup>d</sup> SEP (solar energetic particles), ACR (anomalous cosmic ray), GCR (galactic cosmic ray). 4.6 Gyr exposure is assumed. See Cooper et al. (2003) and Strazzulla et al. (2003).

<sup>e</sup> The assumed origin of these gases is the comet's nuclear ices.

unique hydrogen bonding arrangements. There also exist non-stoichiometric solids with H<sub>2</sub>O/NH<sub>3</sub> ratios different from those of hydrates, and where unique hydrogen bonding does not occur.

Mid-infrared (IR) spectral assignments of all three ammonia hydrates, 2NH<sub>3</sub>·H<sub>2</sub>O, NH<sub>3</sub>·H<sub>2</sub>O, and NH<sub>3</sub>·2H<sub>2</sub>O, have been published for samples authenticated by powder and single-crystal X-ray diffraction studies. Bertie and Morrison (1980) reported IR spectra of 2NH<sub>3</sub>·H<sub>2</sub>O from 2.5 to 25  $\mu$ m, and spectra of NH<sub>3</sub>·H<sub>2</sub>O at 95–100 K from 2.5 to 25  $\mu$ m. Additional features were later identified in the 2- $\mu$ m region (Bertie and Shehata, 1985). The mid-IR spectrum of ammonia dihydrate, NH<sub>3</sub>·2H<sub>2</sub>O, was published by Bertie and Shehata (1984) along with near-IR band positions. In general, each of these hydrates was made from liquid H<sub>2</sub>O + NH<sub>3</sub> mixtures with specific concentrations of NH<sub>3</sub>, cooled and in some cases cycled in temperature. Ammonia hydrates also have been made by gas-phase deposition and subsequent annealing of the individual components, such as in the work of Bertie and Devlin (1984) for 2NH<sub>3</sub>·H<sub>2</sub>O, Sill et al. (1981) for NH<sub>3</sub>·H<sub>2</sub>O, and Huston et al. (1983) for both. In most cases the IR spectra were compared with those of hydrates whose structures had been checked with X-ray diffraction.

Although most of these laboratory spectra were taken in the mid-IR region, spectra of Solar System objects are almost exclusively measured at near-infrared wavelengths where the cold surfaces efficiently reflect solar radiation. Near-IR bands arise from overtones and combinations of a molecule's fundamental vibrations, and typically are an order-of-magnitude weaker than mid-IR features. One of the motivating factors for our present study was to examine in detail the near-IR band positions for NH<sub>3</sub> in hydrates and in icy mixtures to determine any changes with NH<sub>3</sub> concentration or temperature.

A common feature among objects in the outer Solar System is their exposure to particles (mostly H<sup>+</sup>, He<sup>+</sup>, and O<sup>+</sup>) from the solar wind, anomalous cosmic rays, and galactic cosmic rays. For satellites of the giant planets, this exposure is dominated by magnetospheric radiation, which slowly modifies the chemistry of any surface ices present. Table 1 gives estimates of relevant doses and incident fluxes in the outer Solar System, based on the work of Cooper et al. (2003) and Strazzulla et al. (2003). Doses accumulated in 4.6 Gyr by the outer 1 m, 100  $\mu$ m, and 1  $\mu$ m of an ice with an assumed density of 1 g cm<sup>-3</sup> are listed. Objects in a broad zone near 40 AU (i.e., the Pluto system and dynamically cold KBOs) experience moderate irradiation from galactic cosmic-ray ions at micron-to-meter depths. This region is bounded on the sunward side by increasing fluxes of solar energetic ions, resulting in increased surface doses, for example, for centaurs. On the anti-sunward side there are rising fluxes of energetic ions diffusing inward from the termination shock. Table 1 also includes estimates for doses from magnetospheric radiation environments.

Overall, the information in Table 1 suggests that it is important to document the radiation chemistry of frozen NH<sub>3</sub>, both in the presence and absence of H<sub>2</sub>O-ice. Radiation effects will be important for predicting reaction products in outer Solar System ices and for understanding the radiation stability of NH<sub>3</sub>. However, few laboratory experiments have been published on frozen ammonia's radiation chemistry, and none have examined the radiation stability of ammonia hydrates. Strazzulla and Palumbo (1998) irradiated H<sub>2</sub>O + NH<sub>3</sub> ices, condensed at either 10 or 80 K, with 30 keV He<sup>+</sup> ions. The NH<sub>3</sub>/H<sub>2</sub>O ratio decreased as the radiation dose increased at 10 K, and the ratio decreased faster when the experiment was repeated at 80 K. However, Strazzulla and Palumbo (1998) did not separate the NH<sub>3</sub> loss due to sputtering from that due to chemical destruction.

In this paper we consider both the near-IR and mid-IR spectra of various H<sub>2</sub>O-ice mixtures containing NH<sub>3</sub>. Laboratory workers studying ices typically use mid-IR spectroscopy as it is very reliable for determining changes in ice composition and phase with temperature, and in identifying product molecules after energetic processing. This is important in the present paper since one goal is understanding the formation and stability (thermal and radiation) of the NH<sub>3</sub> hydrates. Once a hydrate's identity can be confirmed with known mid-IR spectra, we can extend our measurements into the near-IR to determine band positions and to study the hydrate's thermal evolution and radiation-induced amorphization. A second goal of this paper is to measure the spectral positions of NH<sub>3</sub>-containing ices in the near-IR as a function of concentration in H<sub>2</sub>O, and to document the influence of temperature on these positions. A third focus involves radiation studies of NH<sub>3</sub> in H<sub>2</sub>O ices, including both the identification of products and destruction of NH<sub>3</sub>. Access to many of the spectra presented in this paper is available on the web site: [www-691/gsfsc.nasa.gov/cosmic.ice.lab](http://www-691/gsfsc.nasa.gov/cosmic.ice.lab).

## 2. Experimental methods

Details of our experimental set-ups, cryostats, ice preparation methods, IR spectral measurements, and proton beam source have been published (Moore and Hudson, 1998, 2000; Hudson and Moore, 1995). In brief, ice samples of H<sub>2</sub>O, NH<sub>3</sub>, and mixtures of the two were formed by condensation of gases onto a pre-cooled aluminum mirror at 10–120 K. One set-up used a Bruker Vector 22 spectrometer and the other used a Nicolet Nexus 670 spectrometer to measure ice spectra from 1 to 25 μm before and during processing (thermal and/or radiation). Since the IR beam passed through the ice before and after reflection at the ice-mirror interface, this IR measurement is called transmission–reflection–transmission (TRT). In each system, the ice could be maintained at a temperature between ~10 and 300 K.

To produce icy mixtures of H<sub>2</sub>O and NH<sub>3</sub>, two gas bulbs, one containing H<sub>2</sub>O and the other containing NH<sub>3</sub>, were each connected to separate deposition tubes. Each tube had a calibrated variable leak valve that was set to provide the flow rate needed for the desired ice composition. The flow rates were determined by separate calibration deposits.

A slightly different technique was used for making ammonia hydrates. Typically, the formation of 2NH<sub>3</sub>·H<sub>2</sub>O and NH<sub>3</sub>·H<sub>2</sub>O was achieved by the thermal processing of ices condensed from appropriate mixtures of ammonia and water vapor. Our usual procedure was to deposit a pre-mixed sample with nominal composition H<sub>2</sub>O/NH<sub>3</sub> ≈ 0.5–1. The deposit was made from a bulb very close (~10 cm) to the cryostat's cold-finger since it was found that concentrations of H<sub>2</sub>O–NH<sub>3</sub> mixtures changed significantly if sent through a long run of tubing. The actual H<sub>2</sub>O/NH<sub>3</sub> ratio in an ice sample was determined spectroscopically after the deposit (see below), and was typically 0.3–33. Stable hydrates were only observed in experiments involving ices that ranged from H<sub>2</sub>O/NH<sub>3</sub> ≈ 0.3–1.3. Mixtures

that differed substantially from the correct stoichiometry did not make the hydrates. Depositions were usually performed at 50 or 95 K, and the resulting spectra resembled those of a mixed amorphous-phase ice film of the two components. When such samples were warmed to 130–135 K, characteristic features of 2NH<sub>3</sub>·H<sub>2</sub>O grew in, and when further warmed to ~155 K the IR features of NH<sub>3</sub>·H<sub>2</sub>O emerged, indicating loss of NH<sub>3</sub> from the hydrate. See the next section for spectra and additional details.

Infrared spectra of ices usually were recorded as 100-scan accumulations, typically at a resolution of 4 cm<sup>-1</sup> from 6000–400 cm<sup>-1</sup> (1.67–25 μm). The composition of an ice mixture was determined by calculating the number of molecules of H<sub>2</sub>O and NH<sub>3</sub> present. An IR band's optical density,  $\int \tau(\tilde{\nu}) d\tilde{\nu}$  in cm<sup>-1</sup>, could be converted to a molecular column density  $N$ , in molecules cm<sup>-2</sup> through

$$N = \frac{\int \tau(\tilde{\nu}) d\tilde{\nu}}{A}$$

provided that the band's intrinsic strength,  $A$  in cm molecule<sup>-1</sup>, was known. The mid-IR libration band of H<sub>2</sub>O near 760 cm<sup>-1</sup> (13.1 μm) is not blended with NH<sub>3</sub> bands, and so was used to determine the H<sub>2</sub>O number density in our ices. For the H<sub>2</sub>O libration band,  $A = 2.8 \times 10^{-17}$  cm molecule<sup>-1</sup> (Hudgins et al., 1993). The mid-IR NH<sub>3</sub>  $\nu_2$  “umbrella” mode at 1070 cm<sup>-1</sup> (9.3 μm) was used to determine the column density of NH<sub>3</sub>. The  $A$ -value used for the  $\nu_2$  band of NH<sub>3</sub> was  $1.7 \times 10^{-17}$  cm molecule<sup>-1</sup> (d'Hendecourt and Allamandola, 1986). We assumed that the 80 K  $A$ -values for both H<sub>2</sub>O and NH<sub>3</sub> were the same as those measured at 10 K. Most ice films were several microns in thickness, as determined by a laser interference fringe system.

Some experiments involved radiation processing of samples. In these cases, IR spectra were recorded before and after exposure of ices to a 0.8 MeV proton beam from a Van de Graaff accelerator. The use of proton irradiation to simulate radiation processing of ices in different cosmic environments has been discussed in other papers (e.g., Hudson et al., 2001; Moore et al., 1983). Radiation doses were determined by measuring the proton fluence (p<sup>+</sup> cm<sup>-2</sup>) in the metal substrate beneath the ice sample and then converting to a common scale of eV per 16-amu molecule, referred to in this paper simply as eV molecule<sup>-1</sup>. The eV per 16-amu scale was primarily chosen so that our results could directly be compared with previously published data. Stopping powers were calculated with Ziegler's SRIM program (Ziegler et al., 1985; [www.srim.org](http://www.srim.org)) to be 274 and 344 MeV cm<sup>2</sup> g<sup>-1</sup> for H<sub>2</sub>O and NH<sub>3</sub>, respectively. For the stopping powers of mixtures, we used the weighted average of the H<sub>2</sub>O and NH<sub>3</sub> stopping powers, with the weighting factor taken from the ice's initial H<sub>2</sub>O/NH<sub>3</sub> ratio. A density of 1 g cm<sup>-3</sup> was assumed for all samples.

Reagents used and their purities were as follows: triply-distilled H<sub>2</sub>O with a resistivity greater than 10<sup>7</sup> ohm cm, Matheson anhydrous NH<sub>3</sub> (99.99%), Aldrich ammonium hydroxide (28–30% ammonia), and Merck Sharp and Dohme 98.8% ammonia-<sup>15</sup>N.

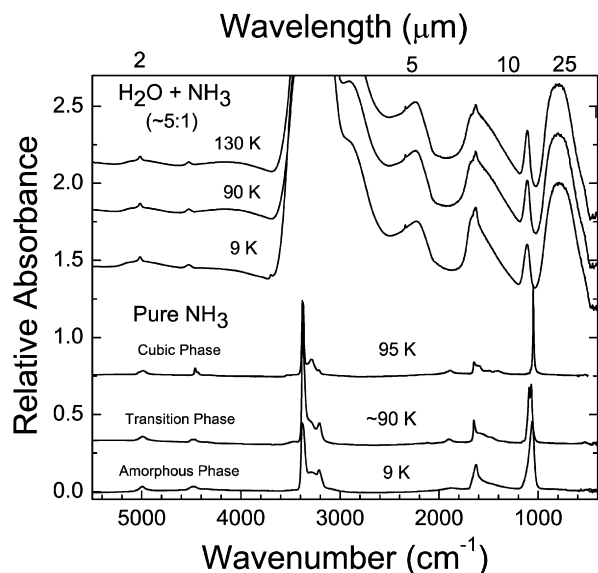


Fig. 1. IR spectra of pure NH<sub>3</sub> compared to IR spectra of H<sub>2</sub>O + NH<sub>3</sub> ices (~5:1). The NH<sub>3</sub> ice was ~1 μm thick and the H<sub>2</sub>O + NH<sub>3</sub> ice was ~5 μm thick. Both ices were made at 9 K and subsequently warmed to the temperatures indicated. Spectra are stacked for clarity.

### 3. Results

#### 3.1. Infrared spectra of NH<sub>3</sub> and H<sub>2</sub>O + NH<sub>3</sub>

Fig. 1 compares IR spectra of deposits of pure NH<sub>3</sub> with those of H<sub>2</sub>O + NH<sub>3</sub> (~5:1). Pure NH<sub>3</sub> deposited at 9 K has absorptions at 3380 ( $\nu_1, \nu_3$ ), 1626 ( $\nu_4$ ), and 1060 ( $\nu_2$ ) cm<sup>-1</sup>. Near-IR bands seen at 4994 cm<sup>-1</sup> and 4478 cm<sup>-1</sup> are assigned as the combination bands ( $\nu_1 + \nu_4$ ) and ( $\nu_1 + \nu_2$ ), respectively (Gerakines et al., 2005). This amorphous NH<sub>3</sub> ice was observed to convert to a transition phase as the ice was warmed from 70 to 90 K. The cubic phase shown in Fig. 1 was formed by directly depositing NH<sub>3</sub> at 95 K, although direct deposit even at 77 K also resulted in cubic-phase NH<sub>3</sub> (Moore and Hudson, 1994). It may be possible to form the cubic phase from the transition phase by a series of thermal annealings, although NH<sub>3</sub> is rapidly lost in our vacuum environment when the temperature is maintained at 120 K. For comparison, Fig. 1 also shows the IR spectrum of a H<sub>2</sub>O + NH<sub>3</sub> mixture (H<sub>2</sub>O/NH<sub>3</sub> = 5) deposited at 9 K, and its change when the ice was warmed to 90 and 130 K.

The weak overtone bands of NH<sub>3</sub> also were seen in H<sub>2</sub>O + NH<sub>3</sub> ices. In the 4000–400 cm<sup>-1</sup> (2.5–25 μm) region, the  $\nu_1$  and  $\nu_3$  bands of H<sub>2</sub>O and NH<sub>3</sub> overlap producing a broad band near 3250 cm<sup>-1</sup> (3.08 μm). Similarly, there is an overlap of the  $\nu_2$  H<sub>2</sub>O and  $\nu_4$  NH<sub>3</sub> bands near 1650 cm<sup>-1</sup> (6.06 μm). Two other broad features of amorphous H<sub>2</sub>O-ice and the  $\nu_2$  bands of NH<sub>3</sub> do not overlap with each other. Band positions for many of these features are listed in Table 2. Neither peak splitting due to the presence of the transition phase of NH<sub>3</sub> at 90 K, nor rapid loss of NH<sub>3</sub> at 130 K was detected in the H<sub>2</sub>O + NH<sub>3</sub> ice mixture warmed to 90 and 130 K.

Table 2

IR band positions, in cm<sup>-1</sup> (μm), of NH<sub>3</sub> and H<sub>2</sub>O + NH<sub>3</sub> ices at different temperatures

Identification	9 K	Pure NH <sub>3</sub>	95 K	H <sub>2</sub> O + NH <sub>3</sub> (~3:1)		
	amorphous	~90 K	cubic	9 K	~90 K	130 K
$\nu_1 + \nu_4$ NH <sub>3</sub>	4994 (2.00)	4989 (2.00)	4989 (2.00)	5013 (1.99)	5013 (1.99)	5013 (1.99)
$\nu_1 + \nu_2$ NH <sub>3</sub>	4478 (2.23)	4474 (2.24)	4461 (2.24)	4525 (2.21)	4524 (2.21)	4525 (2.21)
$\nu_1, \nu_3$ NH <sub>3</sub>	3380 (2.96)	3380 (2.96)	3380 (2.96)			
$\nu_1, \nu_3$ H <sub>2</sub> O and NH <sub>3</sub>	–	–	–	Broad band in the 3250 (3.08) region		
$3\nu_L$ H <sub>2</sub> O	–	–	–	Weak broad band in the 2224 (4.50) region		
$\nu_4$ NH <sub>3</sub>	1649 (6.06)	1626 (6.15)	1649 (6.06)	–	–	–
$\nu_2$ H <sub>2</sub> O, and $\nu_4$ NH <sub>3</sub>	–	–	–	Weak broad H <sub>2</sub> O band in the 1650 (6.06) region with an overlapping NH <sub>3</sub> peak at 1630 (6.13)		
$\nu_2$ NH <sub>3</sub>	1060 (9.43)	1071 (9.34), 1092 (9.16)	1049 (9.53)	1110 (9.01)	1109 (9.02)	1108 (9.03)
$\nu_L$ H <sub>2</sub> O	–	–	–	800 (12.5)	805 (11.8)	818 (12.2)

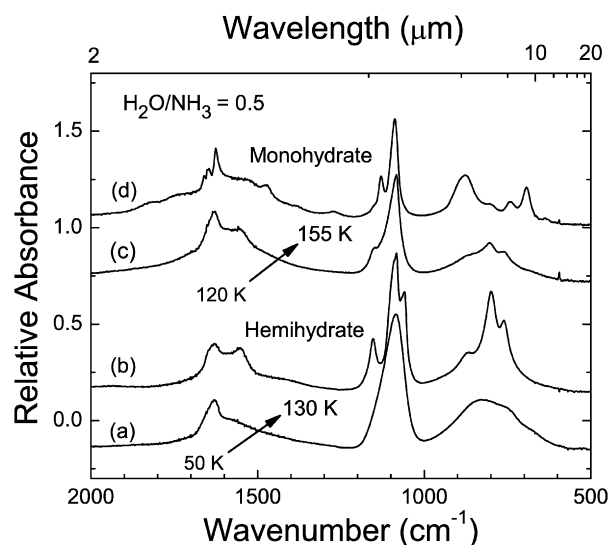


Fig. 2. IR spectra of ices made from H<sub>2</sub>O/NH<sub>3</sub> = 0.5 gas-phase mixtures. Ices made at 50 K formed 2NH<sub>3</sub>·H<sub>2</sub>O after warming to 130 K, while deposits made at 120 K formed NH<sub>3</sub>·H<sub>2</sub>O after warming to 155 K.

#### 3.2. Formation of ammonia hydrates 2NH<sub>3</sub>·H<sub>2</sub>O and NH<sub>3</sub>·H<sub>2</sub>O

Formation of ammonia hemihydrate (2NH<sub>3</sub>·H<sub>2</sub>O) and ammonia hydrate (NH<sub>3</sub>·H<sub>2</sub>O) was observed upon warming ices made by condensation of appropriate gas-phase NH<sub>3</sub>–H<sub>2</sub>O mixtures. Fig. 2 shows spectra of an ice made at 50 K and sub-

Table 3  
IR band positions, in  $\text{cm}^{-1}$  ( $\mu\text{m}$ ), for  $2\text{NH}_3\cdot\text{H}_2\text{O}$  and  $\text{NH}_3\cdot\text{H}_2\text{O}$  at 90–100 K

IR band	$2\text{NH}_3\cdot\text{H}_2\text{O}$		$\text{NH}_3\cdot\text{H}_2\text{O}$	
	This work	Reference <sup>a</sup>	This work	Reference <sup>b</sup>
$\nu_3 + \nu_4$	5009 (2.00)	–	5014 (1.99)	5015 (1.99)
$\nu_3 + \nu_2$	4512 (2.22), 4463 (2.24) sh	–	4518 (2.21)	4515 (2.21)
$\nu_3 \text{ NH}_3$	3397.0 (2.94) vs	3397 (2.94)	3395.0 (2.95) vs	3392.2 (2.95)
$\nu_3 \text{ NH}_3$	3377.5 (2.96) vs	3374 (2.96)	3387.6 (2.95) vs	3387.3 (2.95)
$\nu_1 \text{ NH}_3$ and $2\nu_4 \text{ NH}_3$	–	–	3333.6 (3.00) s	3332 (3.00)
$\nu_{\text{OH}} - \text{O}$	–	–	3273.2 (3.06) vs	3275 (3.05)
$\nu_{\text{OH}} - \text{O}$	–	–	3203.4 (3.12) vs	3182 (3.14)
$\nu_{\text{OH}} - \text{N}'$	3139.6 (3.19) vs	3125 (3.20)	–	–
$\nu_{\text{OH}} - \text{N}$	2995.4 (3.34) vs	2975 (3.36)	2899.3 (3.35) vs	2887 (3.46)
$\nu_4 \text{ NH}_3$ and $\nu_2 \text{ H}_2\text{O}$	1629.6 (6.14) m	1626 (6.15)	1627.3 (6.15) m	1627 (6.15)
$2\nu_{\text{R}} \text{ H}_2\text{O}$	1552.7 (6.44) m	1555 (6.43)	1486.5 (6.73) w	1480 (6.76)
$2\nu_{\text{R}} \text{ H}_2\text{O}$	–	–	1284.2 (7.79) w	1287.1 (7.77)
$\nu_2 \text{ NH}_3$	1154.1 (8.66) m	1156 (8.65)	1129.8 (8.85) s	1133.4 (8.82)
$\nu_2 \text{ NH}_3$	1083.9 (9.23) vs	1083 (9.23)	1102.2 (9.07) vs	1095 (9.13)
$\nu_{\text{R}} \text{ H}_2\text{O}$	–	–	~922 (10.8) s	~932 (10.7)
$\nu_{\text{R}} \text{ H}_2\text{O}$	876.3 (11.4) w	~882 (11.3)	876.7 (11.4) s	~893 (~11.2)
$\nu_{\text{R}} \text{ H}_2\text{O}$	806.2 (12.4) s	817 (12.2)	–	–
$\nu_{\text{R}} \text{ H}_2\text{O}$	763.7 (13.1) m	767 (13.0)	748.5 (13.4) m	~750 (~13.3)
$\nu_{\text{R}} \text{ H}_2\text{O}$	–	–	701.9 (14.2) s	709.9 (14.1)
$\nu_{\text{R}} \text{ H}_2\text{O}$	–	–	642.7 (15.6) m	644.2 (15.5)

<sup>a</sup> 90 K, Bertie and Devlin (1984).

<sup>b</sup> 100 K, Bertie and Shehata (1985).

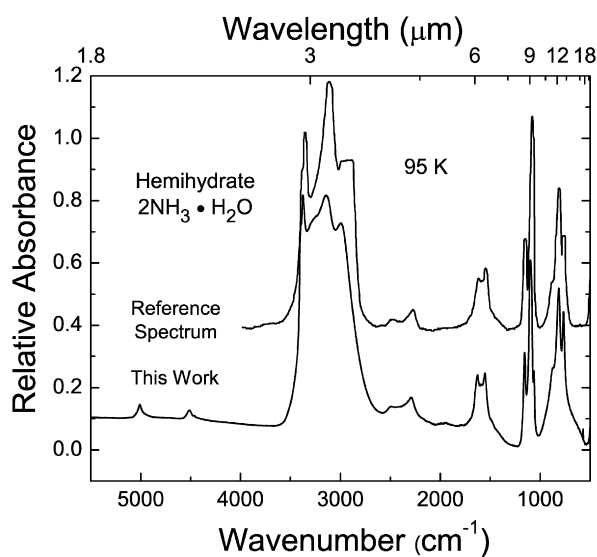


Fig. 3. The IR spectrum of  $2\text{NH}_3\cdot\text{H}_2\text{O}$  formed in this work has weak combination bands near 2.0 and 2.2  $\mu\text{m}$  at 95 K. A reference spectrum of  $2\text{NH}_3\cdot\text{H}_2\text{O}$  is also shown (Bertie and Morrison, 1980).

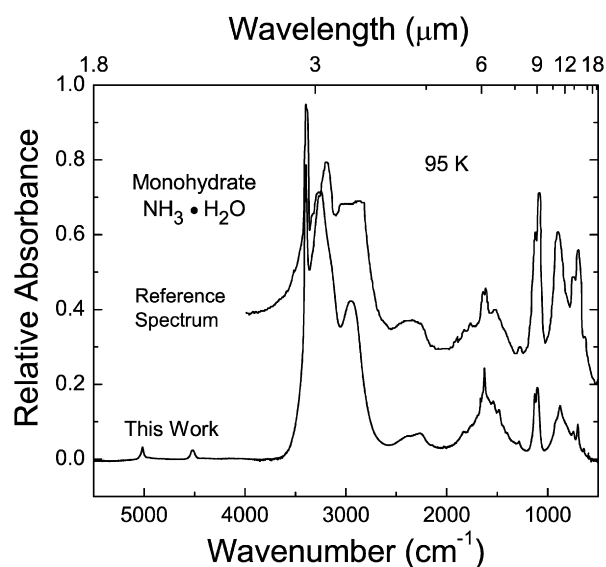


Fig. 4. The IR spectrum of  $\text{NH}_3\cdot\text{H}_2\text{O}$  formed in this work has weak combination bands near 2.0 and 2.2  $\mu\text{m}$  at 95 K. A reference spectrum of  $\text{NH}_3\cdot\text{H}_2\text{O}$  is also shown (Bertie and Morrison, 1980).

sequently warmed to 130 K to form  $2\text{NH}_3\cdot\text{H}_2\text{O}$ . Also shown are spectra of an ice made at 120 K and subsequently warmed to 155 K to make  $\text{NH}_3\cdot\text{H}_2\text{O}$ . Fig. 3 shows the good agreement between our IR spectra and those of Bertie and Morrison (1980) for  $2\text{NH}_3\cdot\text{H}_2\text{O}$ , while Fig. 4 shows similar agreement between our results for  $\text{NH}_3\cdot\text{H}_2\text{O}$  and the spectra of Bertie and Morrison (1980) and Bertie and Shehata (1985). Table 3 compares our peak positions for the major hydrate bands at 95 K with literature values (Bertie and Morrison, 1980; Bertie and Devlin, 1984; Bertie and Shehata, 1985).

When  $2\text{NH}_3\cdot\text{H}_2\text{O}$  was warmed, we observed its conversion to  $\text{NH}_3\cdot\text{H}_2\text{O}$ , along with a loss of  $\text{NH}_3$ . Fig. 5 shows the result of raising the temperature of the hemihydrate under a dynamic vacuum. Spectrum 5a duplicates the  $2\text{NH}_3\cdot\text{H}_2\text{O}$  spectrum of Fig. 2b. Increasing the temperature from the 130–140 K region changed the band intensities by only a small amount. At 150 K the ice spectrum, shown in Fig. 5b, possessed features in the  $800 \text{ cm}^{-1}$  ( $12.5 \mu\text{m}$ ) region characteristic of both  $2\text{NH}_3\cdot\text{H}_2\text{O}$  and  $\text{NH}_3\cdot\text{H}_2\text{O}$ . When the temperature was increased further, to the 155–165 K region, the ice converted

completely into  $\text{NH}_3 \cdot \text{H}_2\text{O}$ . We have some preliminary evidence that this  $2\text{NH}_3 \cdot \text{H}_2\text{O} \rightarrow \text{NH}_3 \cdot \text{H}_2\text{O}$  conversion might occur as low as 145 K, as when we performed slower warmings on one sample, 1:1 hydrate features began to appear after about 50 min at that temperature. (The time scale for most of our warming runs was about 10 min.) This lower conversion temperature is consistent with the observations of [Huston et al. \(1983\)](#). The further thermal evolution of the monohydrate into the dihydrate (32 mass % ammonia),  $\text{NH}_3 \cdot \text{H}_2\text{O} \rightarrow \text{NH}_3 \cdot 2\text{H}_2\text{O}$ , was not seen. Instead, on warming  $\text{NH}_3 \cdot \text{H}_2\text{O}$  to  $\sim 165$  K, its IR bands weakened substantially, leaving a spectrum similar to that of pure  $\text{H}_2\text{O}$  ([Fig. 5d](#)).

We also succeeded in forming the  $2\text{NH}_3 \cdot \text{H}_2\text{O}$  and  $\text{NH}_3 \cdot \text{H}_2\text{O}$  hydrates in another manner, by direct injection of concentrated aqueous ammonia solutions onto a cold substrate with subsequent warming of the ice. When microliter quantities of commercial concentrated  $\text{NH}_3$  solution (from Aldrich) were used, the sample showed little or no sign of the hydrates. However, when the commercial solution was enriched before injection by bubbling  $\text{NH}_3$  gas through it at  $\sim 173$  K, we saw clear IR signals of both  $2\text{NH}_3 \cdot \text{H}_2\text{O}$  (on warming to  $\sim 130$  K) and  $\text{NH}_3 \cdot \text{H}_2\text{O}$  (on warming to  $\sim 150$  K). The reason for “fortifying” the commercial solution was to try to bring the  $\text{NH}_3$  mass percent up from 28–30% (cited by Aldrich) closer to the 32%

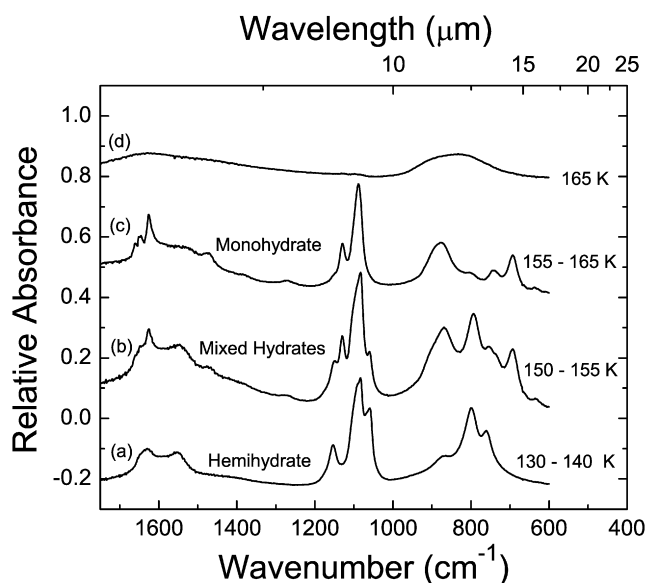


Fig. 5. The thermal evolution of (a)  $2\text{NH}_3 \cdot \text{H}_2\text{O}$  shows loss of  $\text{NH}_3$  to give (b) a mixture of  $2\text{NH}_3 \cdot \text{H}_2\text{O}$  and  $\text{NH}_3 \cdot \text{H}_2\text{O}$  hydrates and then (c) a complete conversion to  $\text{NH}_3 \cdot \text{H}_2\text{O}$ . Additional warming removes the remaining  $\text{NH}_3$ , giving spectrum (d), which is characteristic of  $\text{H}_2\text{O}$ -ice. Spectra are stacked for clarity.

Table 4

Near IR band positions, in  $\text{cm}^{-1}$  ( $\mu\text{m}$ ), of pure  $\text{NH}_3$  compared to  $\text{NH}_3$  in different mixtures at  $\sim 90$  K

$\text{NH}_3$ amorphous phase	$\text{NH}_3$ transition phase	$\text{NH}_3$ cubic phase	$2\text{NH}_3 \cdot \text{H}_2\text{O}$ hemihydrate	$\text{NH}_3 \cdot \text{H}_2\text{O}$ monohydrate	$\text{H}_2\text{O} + \text{NH}_3$ ( $\sim 5:1$ )
4994 (2.00)	4989 (2.00)	4989 (2.00)	5009 (2.00)	5014 (1.99)	5016 (1.99)
4478 (2.23)	4474 (2.24)	4461 (2.24)	4512 (2.22), 4463 (2.24) sh	4518 (2.21)	4527 (2.21)

of the  $\text{NH}_3 \cdot 2\text{H}_2\text{O}$  ammonia dihydrate compound. This enrichment process did result in as much as an 8-fold increase in the proportion of  $\text{NH}_3$  appearing in samples condensed by injection at 50 K. While there were some indications that we might have formed the dihydrate ( $\text{NH}_3 \cdot 2\text{H}_2\text{O}$ ) in these experiments, we could not conclusively identify it. [Bertie and Shehata \(1984\)](#) did publish near-IR band positions for the dihydrate, formed by cooling and temperature cycling appropriate liquid mixtures, and some of their values are included later in this paper for comparison.

[Fig. 6](#) displays near-IR spectra of the amorphous, transition, and cubic phases of pure  $\text{NH}_3$ , spectra of  $2\text{NH}_3 \cdot \text{H}_2\text{O}$ ,  $\text{NH}_3 \cdot \text{H}_2\text{O}$ , and  $\text{H}_2\text{O} + \text{NH}_3$  (5:1) ices, and spectra of pure amorphous-phase  $\text{H}_2\text{O}$ -ice, all in the  $5400\text{--}4000$   $\text{cm}^{-1}$  (1.85–2.5  $\mu\text{m}$ ) region. These ices represent  $\text{NH}_3$  mass percents of 100, 65, 49, 16, and 0, respectively. Band positions for those ices with  $\text{NH}_3$  are listed in [Table 4](#). Small shifts in the hydrate near-IR bands were observed with temperature. The hemihydrate ranged from 5014 and  $4514$   $\text{cm}^{-1}$  (1.99 and 2.22  $\mu\text{m}$ ) at 165 K to 5007 and  $4515$   $\text{cm}^{-1}$  (2.00 and 2.21  $\mu\text{m}$ ) at 10 K; the monohydrate was measured at 5015 and  $4515$   $\text{cm}^{-1}$  at 155 K and 5014 and  $4518$   $\text{cm}^{-1}$  at 95 K.

### 3.3. Near-IR spectra of $\text{H}_2\text{O} + \text{NH}_3$ mixtures

In order to investigate changes in the  $(\nu_1 + \nu_2)$  and  $(\nu_1 + \nu_4)$  bands of  $\text{NH}_3$  as a function of dilution in  $\text{H}_2\text{O}$ , we deposited, at

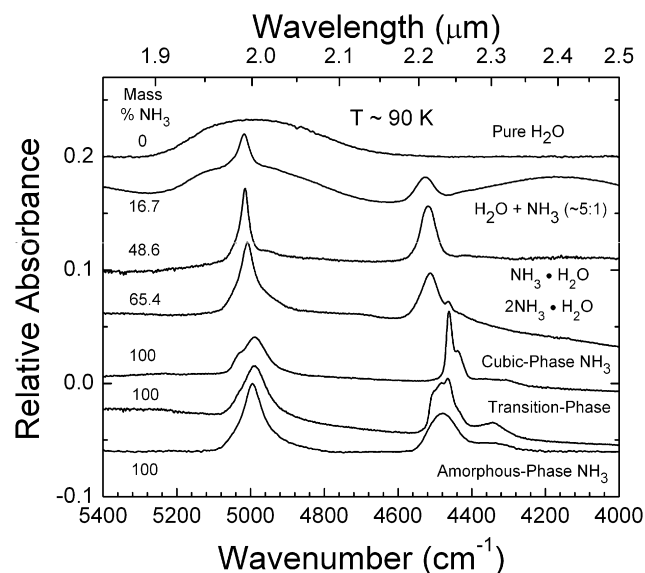


Fig. 6. Near-IR spectra from  $5400$  to  $4000$   $\text{cm}^{-1}$  (1.85–2.5  $\mu\text{m}$ ) of  $2\text{NH}_3 \cdot \text{H}_2\text{O}$  and  $\text{NH}_3 \cdot \text{H}_2\text{O}$  compared to spectra of pure  $\text{NH}_3$  and a  $\text{H}_2\text{O} + \text{NH}_3$  (5:1) mixture.

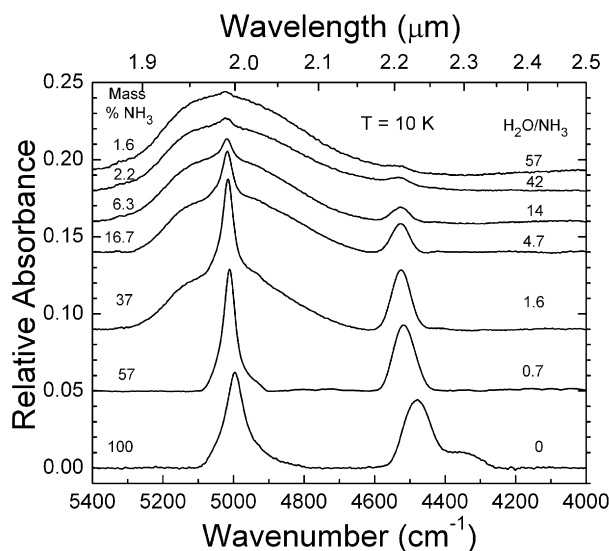


Fig. 7. Near-IR spectrum from 5600 to 4000  $\text{cm}^{-1}$  (1.78–2.5  $\mu\text{m}$ ) of pure amorphous  $\text{NH}_3$  compared to spectra of amorphous ice mixtures with  $\text{H}_2\text{O}/\text{NH}_3$  ratios equal to 0.7, 1.6, 4.7, 14, 42, and 57, all at 10 K.

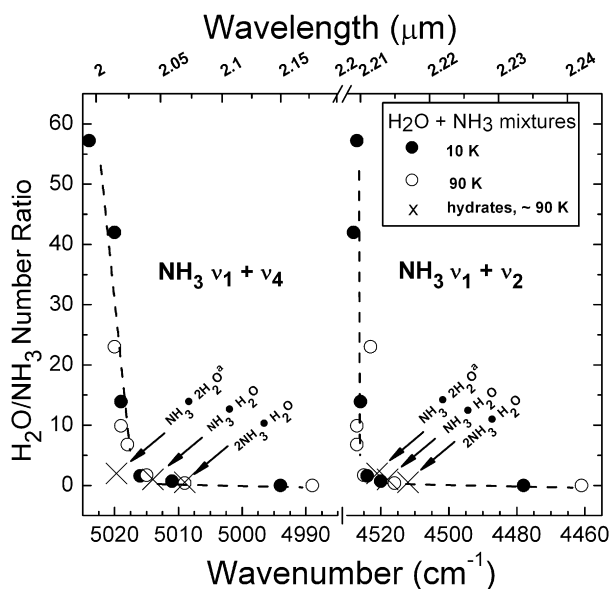


Fig. 8. Positions of the  $(\nu_1 + \nu_2)$  and  $(\nu_1 + \nu_4)$  bands of  $\text{NH}_3$  as a function of the  $\text{H}_2\text{O}/\text{NH}_3$  ratio for ices formed at 10 and 90 K. Positions for the three  $\text{NH}_3$  hydrates at 90 K are included for comparison, with the dihydrate data being taken from Bertie and Shehata (1984).

10 and 90 K, gaseous mixtures with a variety of  $\text{H}_2\text{O}/\text{NH}_3$  ratios. Fig. 7 shows the 5400 to 4000  $\text{cm}^{-1}$  (1.85–2.5  $\mu\text{m}$ ) region for pure  $\text{NH}_3$  and  $\text{H}_2\text{O} + \text{NH}_3$  mixtures having  $\text{H}_2\text{O}/\text{NH}_3 = 0.7, 1.6, 4.7, 14, 42,$  and 57, all deposited at 10 K. Ices used for the spectra in Fig. 7 were typically 20  $\mu\text{m}$  thick. The  $\text{H}_2\text{O}/\text{NH}_3$  ratio was determined early in the deposit using ice thicknesses no larger than 2  $\mu\text{m}$ . Both near-IR bands of  $\text{NH}_3$  were detected in even the most dilute ice. No apparent change in the relative intensity of one  $\text{NH}_3$  near-IR band compared to the other was obvious with dilution.

Fig. 8 shows changes in the peak positions of the two near-IR ammonia bands with dilution for both 10 and 90 K deposits.

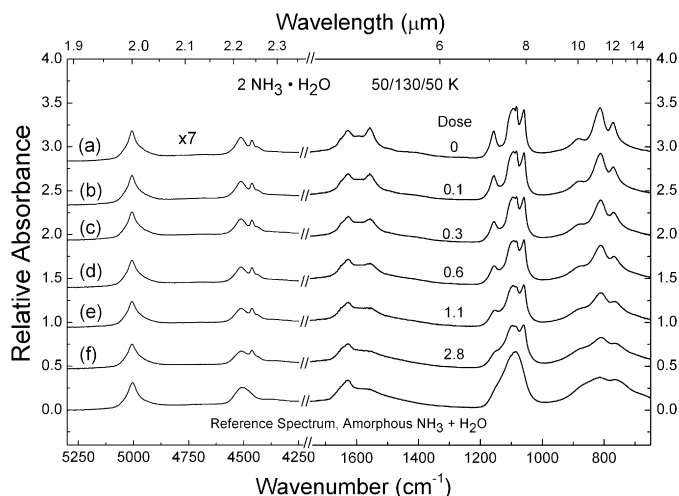


Fig. 9. Changes in the near- and mid-IR spectrum of  $2\text{NH}_3 \cdot \text{H}_2\text{O}$  at 50 K as a function of radiation dose.

In general, there is overlap between the data sets for the two temperatures. A few dashed lines have been added to Fig. 8 to help guide the eye. This figure shows that the largest influence on band positions was ice composition and not temperature. Here a clear tendency is seen for both bands to shift to larger wavenumbers as  $\text{NH}_3$  becomes more diluted in the  $\text{H}_2\text{O}$ -ice. (For  $\text{H}_2\text{O}/\text{NH}_3 = 0$ , we used the band position for cubic-phase  $\text{NH}_3$  deposited at 90 K listed in Table 2.) The largest wavenumber shift for the 10 K data occurs for  $\text{H}_2\text{O}/\text{NH}_3$  ratios from 0 to  $\sim 2$  where the band position for shifts  $\sim 46 \text{ cm}^{-1}$  for  $(\nu_1 + \nu_2)$  and  $\sim 22 \text{ cm}^{-1}$  for  $(\nu_1 + \nu_4)$ , both to larger wavenumbers. The shifts for the 90 K data are greater because the positions for the  $\text{H}_2\text{O}/\text{NH}_3 = 0$  ice occurs at smaller wavenumbers for both bands. In the 90 K case the shift is  $\sim 64 \text{ cm}^{-1}$  for  $(\nu_1 + \nu_2)$  and  $\sim 26 \text{ cm}^{-1}$  for  $(\nu_1 + \nu_4)$  again to larger wavenumbers. Continuing to the more dilute mixtures we tested, the  $(\nu_1 + \nu_4)$  band continues to move to slightly larger wavenumbers, approximately another  $5 \text{ cm}^{-1}$  between  $\text{H}_2\text{O}/\text{NH}_3 \sim 2$  and 60, whereas the  $(\nu_1 + \nu_2)$  band's position remains about the same. For comparison in Fig. 8, our positions for the mono- and dihydrates at 95 K are indicated as is the position of the dihydrate reported by Bertie and Shehata (1984). This plot shows that almost no change in the  $\text{NH}_3$  near-IR band positions occurs beyond a  $\text{H}_2\text{O}/\text{NH}_3$  ratio of about 3, and that the band positions of all hydrates fall essentially on the same curve as the amorphous  $\text{H}_2\text{O} + \text{NH}_3$  mixtures.

### 3.4. IR spectra and radiation effects in hydrates and $\text{H}_2\text{O} + \text{NH}_3$ icy mixtures

#### 3.4.1. Amorphization of $2\text{NH}_3 \cdot \text{H}_2\text{O}$

Fig. 9a shows the near- and mid-IR spectrum of the hemihydrate at 50 K before and after irradiation. Its temperature history is written 50/130/50 to indicate that the ice was condensed at 50 K, warmed to 130 K to form  $2\text{NH}_3 \cdot \text{H}_2\text{O}$ , and then recooled to 50 K for irradiation. Proton irradiation of this crystalline solid caused its unique mid-IR absorptions to become less intense as the radiation dose increased (Figs. 9b–9f).

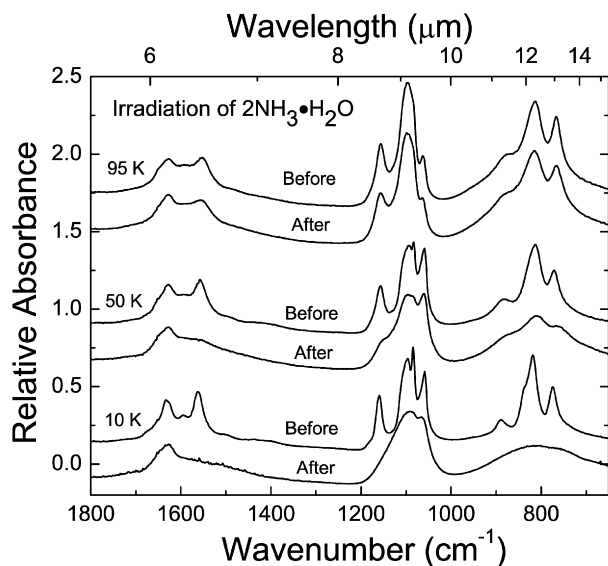


Fig. 10. Changes in the IR spectrum of  $2\text{NH}_3 \cdot \text{H}_2\text{O}$  before and after an irradiation of  $\sim 2.8 \text{ eV molecule}^{-1}$ . The irradiation temperatures were 95, 50, and 10 K.

After a total dose of  $2.8 \text{ eV molecule}^{-1}$ , the resulting spectrum (9f) was similar to a reference spectrum of the originally-deposited amorphous ice at 50 K (before annealing to form the hydrate). Fig. 10 shows that the effect of  $2.8 \text{ eV molecule}^{-1}$  was even more pronounced when the irradiation was performed at 10 K, while this same dose at 95 K had almost no effect on the spectrum of  $2\text{NH}_3 \cdot \text{H}_2\text{O}$ . To help quantify these effects, we plotted the normalized band area of the  $1100 \text{ cm}^{-1}$  complex of  $2\text{NH}_3 \cdot \text{H}_2\text{O}$  with dose. At 10 K the band area was reduced 40% after  $\sim 8 \text{ eV molecule}^{-1}$ , but the same dose at 95 K reduced the band area by only 15%, as seen in Fig. 11. These results are reminiscent of the radiation-induced amorphization of crystalline  $\text{H}_2\text{O}$ -ice, since in all cases the amorphization rate increases as the temperature decreases (Moore and Hudson, 1992; Baratta et al., 1991; Strazzulla et al., 1991; Mastrapa and Brown, 2006). Also, both crystalline  $\text{H}_2\text{O}$ -ice and  $2\text{NH}_3 \cdot \text{H}_2\text{O}$  (amorphized at either 50 or 10 K) reform when the irradiated ice is warmed. Additional warming of irradiated  $2\text{NH}_3 \cdot \text{H}_2\text{O}$  also led to the  $2\text{NH}_3 \cdot \text{H}_2\text{O} \rightarrow \text{NH}_3 \cdot \text{H}_2\text{O}$  conversion in all cases.

#### 3.4.2. Loss of ammonia during irradiation

Ammonia destruction was measured as a function of the initial  $\text{H}_2\text{O}/\text{NH}_3$  ratio in ices proton-irradiated at 10 and at 80 K. Fig. 11 plots the normalized area of the  $\text{NH}_3 \nu_2$  ( $1115 \text{ cm}^{-1}$ ) band as a function of radiation dose. At the top, Fig. 11a shows that at 10 K the rate of decrease of this band depends on the initial  $\text{H}_2\text{O}/\text{NH}_3$  ratio. The loss of band area was proportional to the original  $\text{NH}_3$  column density, decreasing by  $\sim 20$ , 30, and 40% after  $8 \text{ eV molecule}^{-1}$  for  $\text{H}_2\text{O}/\text{NH}_3 = 2$ , 7, and 18, respectively. These results, when compared to those in Fig. 11a for pure  $\text{NH}_3$ , show that radiation chemical destruction of  $\text{NH}_3$  is enhanced when water-ice is present. The 10 K results from three amorphous  $\text{H}_2\text{O}$ - $\text{NH}_3$  mixtures also contrast with the radiation destruction of  $2\text{NH}_3 \cdot \text{H}_2\text{O}$ . The larger decrease in the

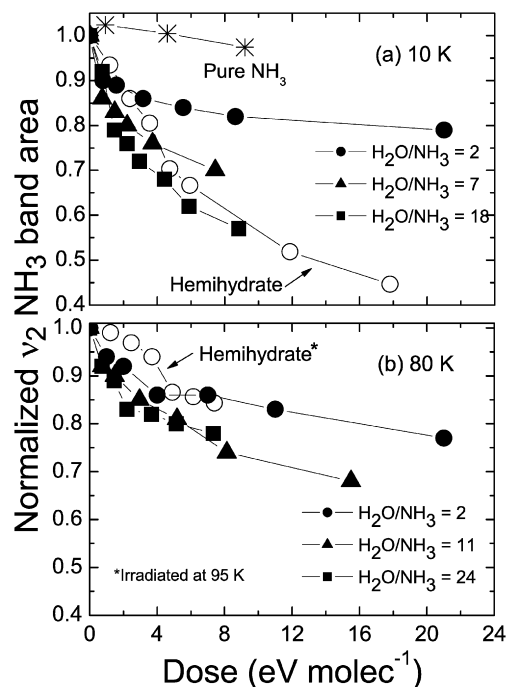


Fig. 11. Changes in the normalized  $\nu_2$   $\text{NH}_3$  band area as a function of dose using 0.8 MeV protons. Changes are plotted for ices with different ice compositions formed and irradiated at both 10 and 80 K. The normalized change in the same band for  $2\text{NH}_3 \cdot \text{H}_2\text{O}$  irradiated at 10 and 95 K is shown for comparison.

hydrate's band area is explained as a combination of ammonia's amorphization and chemical destruction. Moving to the lower half of Fig. 11, the results show that at the higher radiation temperature, 80 K,  $\text{NH}_3$  destruction is similar for amorphous mixtures with different  $\text{H}_2\text{O}/\text{NH}_3$  ratios (Fig. 11b). After a dose of  $\sim 8 \text{ eV molecule}^{-1}$  at 80 K, the  $\text{NH}_3$  band area has decreased by  $\sim 20\%$  for each mixture. A similar decrease is seen in Fig. 11b for the radiation destruction of  $2\text{NH}_3 \cdot \text{H}_2\text{O}$  at 95 K. The decrease in the hydrate's  $\text{NH}_3$  band at this temperature is dominated by chemical destruction.

The change in the  $\text{NH}_3$ -to- $\text{H}_2\text{O}$  molecular number ratio as a function of radiation dose can be calculated from intrinsic band strengths and integrated band areas. Fig. 12 follows the decrease in this ratio, as a function of dose, for ice mixtures deposited at both 10 and 80 K, and having an initial  $\text{H}_2\text{O}/\text{NH}_3$  ratio of 2. For this figure we intentionally use the reciprocal value,  $\text{NH}_3/\text{H}_2\text{O}$ , in order to compare with the results of Strazzulla and Palumbo (1998) on similar  $\text{H}_2\text{O} + \text{NH}_3$ , sub-micron thick ice films irradiated with 30-keV helium ions. The two sets of data clearly show the same trends, with both giving a steeper decrease at 80 than at 10 K. Although Strazzulla and Palumbo (1998) did not separate the loss of ammonia's band area due to chemical alteration from the contribution due to sputtering, our results agree with theirs, and we know that MeV proton bombardment is dominated by chemical alteration. (See Section 4.3.2.) From Fig. 12 we can estimate that over  $10^9$  years, similar ices on Charon lose more than 50% of their original ammonia due to radiation chemical processes.

### 3.4.3. Radiation products

Several icy mixtures with different initial  $\text{H}_2\text{O}/\text{NH}_3$  ratios were irradiated at 10 and 80 K, and here we use one ice to demonstrate the changes observed in all of the mixtures. Fig. 13 shows the IR spectrum of an ice, initially having  $\text{H}_2\text{O}/\text{NH}_3 = 7$ , at 10 K before and after a radiation dose of  $7 \text{ eV molecule}^{-1}$ .

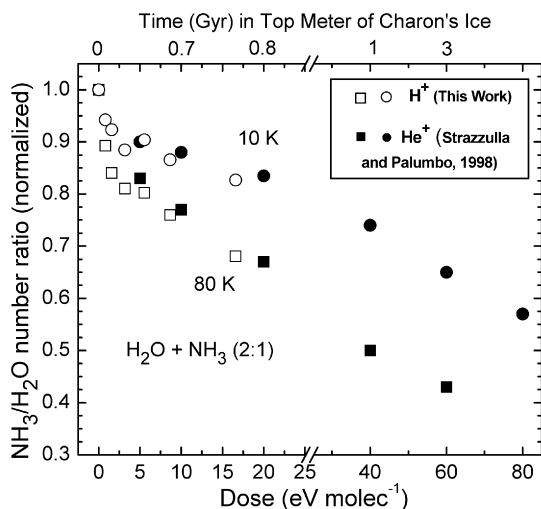


Fig. 12. Changes in the normalized  $\text{NH}_3/\text{H}_2\text{O}$  molecular number ratio as a function of dose using 0.8 MeV protons. Ices were formed and irradiated at both 10 and 80 K, and results are compared in similar ices bombarded with helium ions (Strazzulla and Palumbo, 1998). Two different horizontal scales are used to show details at low dose as well as the overall trend at high dose.

The  $\text{NH}_3 \nu_2$  band area was about 30% less after irradiation. The sequential decrease of the  $\nu_2$  band after small irradiation steps is indicated in the inset spectra. Fig. 13 also shows the new absorption feature found at  $1506 \text{ cm}^{-1}$  ( $6.4 \mu\text{m}$ ) after irradiation, which is attributed to the  $\text{NH}_4^+$  ion (ammonium). This ion was identified by comparison with an IR reference spectrum of  $\text{NH}_4^+$  at 10 K, formed by the acid–base reaction between  $\text{HNCO}$  and  $\text{NH}_3$ . Other  $\text{NH}_4^+$  bands were not detected, but the strongest features of  $\text{NH}_4^+$  overlap with the intense  $3.1\text{-}\mu\text{m}$  band of  $\text{H}_2\text{O}$ -ice. Weaker  $\text{NH}_4^+$  overtones at  $2.21$  and  $2.24 \mu\text{m}$  are estimated to be  $\sim 200$  and  $\sim 400$  times less intense, respectively, than the  $6.4\text{-}\mu\text{m}$  band (Moore et al., 2003). Preliminary experiments in our laboratory suggest that the mid-IR bands of  $\text{NH}_4^+$  shift with a dependence on the counterion and matrix material, and so further experiments to examine possible changes in this band's near-IR features are planned.

## 4. Discussion

### 4.1. Formation and thermal evolution of $2\text{NH}_3 \cdot \text{H}_2\text{O}$ and $\text{NH}_3 \cdot \text{H}_2\text{O}$

We have observed the formation of  $2\text{NH}_3 \cdot \text{H}_2\text{O}$  and  $\text{NH}_3 \cdot \text{H}_2\text{O}$  by warming samples made by gas deposition, resulting in ice mixtures ranging from  $\text{H}_2\text{O}/\text{NH}_3 = 0.34$  to  $0.85$  ( $73.7$  to  $52.5$  mass %  $\text{NH}_3$ , respectively), and by injection of aqueous ammonia solutions, resulting in ice mixtures of composition  $\text{H}_2\text{O}/\text{NH}_3 = 0.28$ – $5.81$  ( $77.1$ – $13.8$  mass %  $\text{NH}_3$ , respectively). We were unsuccessful in forming ammonia dihy-

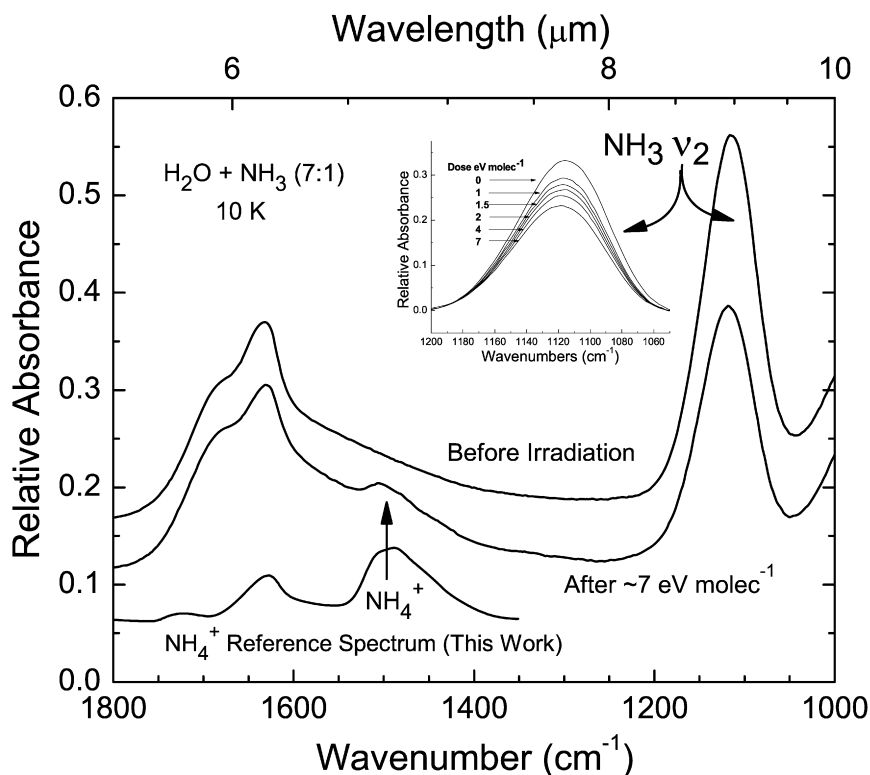


Fig. 13. IR spectra of an  $\text{H}_2\text{O} + \text{NH}_3$  (7:1) ice at 10 K before and after irradiation to a dose of  $7 \text{ eV molecule}^{-1}$ . The incremental decrease in the  $\text{NH}_3 \nu_2$  band is shown in the inset. The formation of  $\text{NH}_4^+$  is identified by comparison with a reference spectrum (see text).

hydrate,  $\text{NH}_3 \cdot 2\text{H}_2\text{O}$ , by warming ices made either by injection or by direct gas deposition. These observations are generally in accord with the water–ammonia low temperature phase diagram (Kargel, 1992; Leliwa-Kopystyński, 2002). In all cases, the sample initially formed was an amorphous mixture of water and ammonia ices. Warming permitted reorganization within the film. Gas depositions that were successful in forming the hydrates all began with ice films at compositions above  $\sim 45$  mass %  $\text{NH}_3$ . Ices or melts above this composition can lead to solid solutions containing the hemihydrate and monohydrate when equilibrium is attained. The hemihydrate appeared easier to form, presumably because a larger range of compositions can lead towards formation of that compound, although  $\text{NH}_3 \cdot \text{H}_2\text{O}$  was formed directly on occasion. Typically, warming was required to convert  $2\text{NH}_3 \cdot \text{H}_2\text{O}$  into  $\text{NH}_3 \cdot \text{H}_2\text{O}$ , since that permitted a change in the bulk composition of the sample; as the more volatile material was lost, the percent of  $\text{NH}_3$  in the sample decreased. That we could not effect complete conversion of  $2\text{NH}_3 \cdot \text{H}_2\text{O}$  to  $\text{NH}_3 \cdot \text{H}_2\text{O}$  in some cases, and never to  $\text{NH}_3 \cdot 2\text{H}_2\text{O}$ , is understandable, since our thin-film ices, open to the vacuum, could not withstand the high temperatures ( $>176$  K) required for melting and the substantial change in the composition of the melt to permit conversion to the lower mass % hydrate. With the relatively slow cooling rate of our cryostats, ices at high temperatures were largely or completely sublimed before they could be recooled. Curiously, ices formed by injection of liquid solutions, even with appropriately low mass %  $\text{NH}_3$ , showed no spectroscopic evidence for the formation of ammonia dihydrate. Rather, the spectra of most of these samples appeared as water ice with trapped  $\text{NH}_3$ . The cooling of these liquid samples immediately upon injection was clearly a non-equilibrium process, and so their behavior is not in accord with published phase diagrams. Further evidence of this is that a small number of such samples, even with low wt%  $\text{NH}_3$ , could be annealed to produce weak signals of the mixed hemi- and monohydrates. Presumably the amorphous solid originally formed had a non-uniform distribution of  $\text{NH}_3$ , and pockets of the appropriate composition behaved as expected with thermal treatment.

#### 4.2. Near-IR bands of $\text{NH}_3$ : Hydrate vs mixture

The most unique spectroscopic features of the ammonia hydrates occur in the mid-IR spectral region. In the near-IR we measured two bands of the hydrates, whose positions had the same values as bands for  $\text{H}_2\text{O} + \text{NH}_3$  ices with the same  $\text{H}_2\text{O}/\text{NH}_3$  ratio. In the near-IR the only feature of these hydrates that was different from  $\text{NH}_3\text{--H}_2\text{O}$  ices was the shoulder at  $4463\text{ cm}^{-1}$  ( $2.24\text{ }\mu\text{m}$ ) for the hemihydrate. However, this shoulder had the same position as pure cubic-phase  $\text{NH}_3$  at 90 K, and is simply residual  $\text{NH}_3$ . Therefore, in the near-IR, we cannot use band positions alone to distinguish between the stoichiometric hydrates and icy mixtures with the same  $\text{NH}_3$  concentration.

The major shifts in the band positions of amorphous  $\text{H}_2\text{O} + \text{NH}_3$  ices occur with changes in concentration. Figs. 6, 7, and 8 document the movement to larger wavenumbers as  $\text{NH}_3$  be-

comes more diluted. Qualitatively, the relative intensities of the  $(\nu_1 + \nu_2)$  and  $(\nu_1 + \nu_4)$  features are similar, based on the observation that both bands appear to diminish equally in intensity with dilution and both are detected for mixtures where  $\text{NH}_3$  is only  $\sim 1.6\%$  abundant (Fig. 7). Attempts to compare integrated band areas were hindered by the fact that the  $(\nu_1 + \nu_4)$  band was blended with the  $2\text{-}\mu\text{m}$  water band.

Band widths for the hemihydrate and monohydrate were measured at 95 K and are listed below. The average of two sets of data was used for the hemihydrate. The average FWHM for amorphous water ice mixtures ( $\text{NH}_3/\text{H}_2\text{O} = 1.17$  and  $1.8$ ) deposited at 50 K is also listed below for comparison. The ratio of the  $\text{FWHM}_{2.2\text{ }\mu\text{m}}/\text{FWHM}_{2\text{ }\mu\text{m}}$  for both the hydrates and the icy mixtures are somewhat different. In all cases the  $2.2\text{ }\mu\text{m}$  band is found to be broader than the  $2\text{ }\mu\text{m}$  band, but the ratio is difficult to quantify based on the number of samples that we have. For example, the average ratio of 6 amorphous deposits with  $\text{H}_2\text{O}/\text{NH}_3$  ratios from  $0.4\text{--}1.6$  (2 and 10 K, 2 and 50 K and 2 and 80 K) is  $2.0 \pm 0.5$ . Typically band shapes for the hydrates were fitted using Lorentzian peak functions, icy mixtures were more Gaussian in shape:

	$\text{FWHM}_{2\text{ }\mu\text{m}}$	$\text{FWHM}_{2.2\text{ }\mu\text{m}}$	$\text{Ratio}_{2.2\text{ }\mu\text{m}/2\text{ }\mu\text{m}}$
Hemihydrate, 95 K	$0.0199 \pm 0.0004\text{ }\mu\text{m}$	$0.0301 \pm 0.0002\text{ }\mu\text{m}$	1.2
Monohydrate, 95 K	$0.0105\text{ }\mu\text{m}$	$0.0235\text{ }\mu\text{m}$	2.2
Icy mixture, 50 K	$0.0212 \pm 0.0011\text{ }\mu\text{m}$	$0.0390 \pm 0.0020\text{ }\mu\text{m}$	1.8

Estimates of the  $A$ -values of the hemihydrate and monohydrate were made for both the  $2$  and  $2.2\text{ }\mu\text{m}$  bands. These were calculated assuming that all of the original  $\text{NH}_3$  underwent complete stoichiometric conversion from the original amorphous ice to the hemihydrate, and from the hemihydrate to the monohydrate. Therefore the values are upper limits. For the hemihydrate, 6 sets of data were used and the results given are consistent to within about 12%. Fewer data sets underwent complete conversion from the hemi- to the monohydrate and those values are less secure. The  $A$ -values are:

	$A_{2\text{ }\mu\text{m}}\text{ (cm molecule}^{-1}\text{)}$	$A_{2.2\text{ }\mu\text{m}}\text{ (cm molecule}^{-1}\text{)}$
Hemihydrate	$2.4 \times 10^{-18}$	$1.8 \times 10^{-18}$
Monohydrate	$2 \times 10^{-18}$	$2 \times 10^{-18}$

#### 4.3. Irradiated ices containing $\text{NH}_3$

##### 4.3.1. Amorphization of $2\text{NH}_3 \cdot \text{H}_2\text{O}$

It is not surprising that  $2\text{NH}_3 \cdot \text{H}_2\text{O}$ , a crystalline material, can be amorphized by ion irradiation at 10 K. Proton irradiation, electron irradiation,  $\text{He}^+$  bombardment, and UV photolysis have all been reported to amorphize crystalline  $\text{H}_2\text{O}$ -ice (see Hudson and Moore, 1995, and references therein). In each of these cases, and in the present work, the dose needed to amorphize the ice sample varies directly with temperature. This similarity between  $2\text{NH}_3 \cdot \text{H}_2\text{O}$  and crystalline  $\text{H}_2\text{O}$ -ice also extends to the observation that once amorphized, the crystalline structure reforms on warming. When  $2\text{NH}_3 \cdot \text{H}_2\text{O}$  was irradiated

at 95 K, the loss rate of the  $\text{NH}_3$   $\nu_2$  ( $1115\text{ cm}^{-1}$ ) band's area was noticeably smaller than at 10 K for the same dose (Fig. 11). The band's decrease was dominated by the radiation-chemical destruction of  $\text{NH}_3$  at 95 K and was similar to that an icy mixture with approximately the same  $\text{NH}_3/\text{H}_2\text{O}$  ratio.

Applying these laboratory results to icy Solar System surfaces requires knowledge of both temperatures and radiation environments, to predict the stability of the  $\text{NH}_3$  hydrate. Using Charon as an example, the surface temperature is near 50 K (e.g., Cook et al., 2007). Our work shows that crystalline features of an ammonia hydrate on Charon's surface will be significantly changed with  $2.5\text{ eV molecule}^{-1}$ , a dose accumulated in an estimated 25 million years.

#### 4.3.2. Loss of $\text{NH}_3$ in irradiated $\text{H}_2\text{O} + \text{NH}_3$ ices

Fig. 11 shows the decrease in the normalized  $\text{NH}_3$  column density with different  $\text{H}_2\text{O}/\text{NH}_3$  ice ratios at two different temperatures. This plot demonstrates that the loss of  $\text{NH}_3$  from irradiated ice is dependent on the  $\text{NH}_3$  concentration at 10 K, but no clear concentration dependence exists at 80 K. At 10 K the most dilute mixture ( $\text{H}_2\text{O}/\text{NH}_3 = 18$ ) had  $\sim 5\%$   $\text{NH}_3$  which was reduced to  $\sim 2.5\%$  after  $9\text{ eV molecule}^{-1}$ . The increased loss of  $\text{NH}_3$  with increasing amounts of  $\text{H}_2\text{O}$  shows that instead of protecting the  $\text{NH}_3$ , irradiated  $\text{H}_2\text{O}$  is a rich source of reactive species that destroy it.

Comparing ices with similar ratios irradiated at different temperatures, the decrease in the normalized  $\text{NH}_3/\text{H}_2\text{O}$  ratio has an initial rapid drop followed by a slower rate of change. The loss rate, however, was larger when the mixture was irradiated at 80 K compared to 10 K. This trend (80 K loss > 10 K loss) was established for doses in the  $10\text{--}15\text{ eV molecule}^{-1}$  range measured in this work and in the work of Strazzulla and Palumbo (1998). The trend continues for doses as high as  $60\text{--}80\text{ eV molecule}^{-1}$ , where an 80 K ice loses  $\sim 60\%$   $\text{NH}_3$  (Strazzulla and Palumbo, 1998).

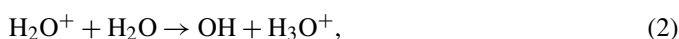
The reduction we observed in the IR features of  $\text{NH}_3$  on irradiation by 0.8 MeV protons is almost entirely from reactions that destroy  $\text{NH}_3$  molecules, and these will be explored in the following section. Another conceivable way for  $\text{NH}_3$  to be lost is by sputtering from the ice sample during proton irradiation. Brown et al. (1982) have shown that the sputtering loss caused by 0.8 MeV protons bombarding  $\text{H}_2\text{O}$ -ice is  $\sim 0.2\text{H}_2\text{O}$  molecules per incident proton, and Johnson et al. (1983) give the  $\text{NH}_3$  loss as eighteen times greater. Based on this information we estimate that only 0.4% of the  $\text{NH}_3$  and 0.01% of the  $\text{H}_2\text{O}$  lost during our dose of  $18\text{ eV molecule}^{-1}$  is due to sputtering. The work of Strazzulla and Palumbo (1998) was done with 30 keV  $\text{He}^+$  ions. Although  $\text{He}^+$  ions have about 3.5 times the sputtering rate of 0.8 MeV  $\text{H}^+$ , the higher electronic stopping power of  $\text{He}^+$  means that only about half as many ions are required to deposit the same energy as our protons. A rough estimate is that the  $\text{NH}_3/\text{H}_2\text{O}$  ratio (for a  $0.2\text{ }\mu\text{m}$  ice) would decrease a few percent due to 30 keV  $\text{He}$  sputtering after  $18\text{ eV molecule}^{-1}$ . The 15% decrease shown in Fig. 12 is consistent with the idea that chemical destruction plays a major role in loss of  $\text{NH}_3$  in both  $\text{H}^+$  and  $\text{He}^+$  experiments. Also,

preferential loss of  $\text{NH}_3$  due to thermal processes does not become significant until temperatures above 130 K are reached.

#### 4.4. Reactions and mechanisms

The primary action of the incident 0.8 MeV protons in our radiation experiments is to cause ionizations and excitations among the reactant molecules. Each high-energy ion travels through the ice sample, producing thousands of secondary electrons indiscriminately from either  $\text{H}_2\text{O}$  or  $\text{NH}_3$ , and leaving a trail of chemical change that includes free radicals, ions, and neutral molecules. The typical path of these secondary electrons is submicrons in length. In this way, it is the abundant secondaries ( $E \sim \text{eV}$  to  $\text{keV}$ ), and not the incident MeV protons, that bring about the bulk of the chemical and physical changes observed.

The radiation chemistry of  $\text{H}_2\text{O}$ -ice has been described both in our own papers (Hudson et al., 2001) and in standard works (Spinks and Woods, 1990; Swallow, 1973). In brief, a secondary (ejected) electron produced by an incident proton will ionize an  $\text{H}_2\text{O}$  molecule to form a radical cation,  $\text{H}_2\text{O}^+$ , which will undergo rapid proton transfer to form a hydronium ion ( $\text{H}_3\text{O}^+$ ) and a hydroxyl radical ( $\text{OH}$ ). Dimerization of  $\text{OH}$  radicals will produce  $\text{H}_2\text{O}_2$ . The relevant reactions are as follows:



In pure water, the fates of the electron in reaction (1) include neutralization by a cation, capture by  $\text{H}_2\text{O}$ , reaction with  $\text{OH}$  to make  $\text{OH}^-$ , and trapping in the ice. Other reaction products that have been reported for the radiolysis of  $\text{H}_2\text{O}$ -ice include  $\text{O}_2$ ,  $\text{H}_2$ , and  $\text{HO}_2$ . In experiments such as ours, using IR spectroscopy as the analytical technique,  $\text{H}_2\text{O}_2$  is the only readily-detectable product molecule (Hudson and Moore, 2006; Loeffler et al., 2006a; Moore and Hudson, 2000).

Reactions similar to the above will apply to pure  $\text{NH}_3$ , with  $\text{NH}_4^+$  being the cation expected. The expected sequence is as follows:



Dimerization of  $\text{NH}_2$  radicals should produce hydrazine ( $\text{N}_2\text{H}_4$ ), but this has not yet been confirmed by low-temperature irradiation of ices. The most likely counter-ion for  $\text{NH}_4^+$  in our  $\text{NH}_3$  experiments is  $\text{N}_3^-$ , which we have observed both in irradiated  $^{14}\text{NH}_3$  and irradiated  $^{15}\text{NH}_3$ , with the expected isotopic shift (Theophanides and Turrell, 1967). The formation pathway for  $\text{N}_3^-$  is uncertain, but this anion's presence strongly hints at  $\text{N}_2$  as a decomposition product in irradiated  $\text{NH}_3$ -ice. Some  $\text{H}_2$  is also expected as a product, but it is not readily detected with IR spectroscopy.

In mixtures of  $\text{H}_2\text{O}$  and  $\text{NH}_3$ , the latter's greater basicity will result in formation of  $\text{NH}_4^+$  at the expense of  $\text{H}_3\text{O}^+$ . Ammonium was, in fact, expected to be the only easily-detected

product, and this was born out by our experiments. All other radiation products from H<sub>2</sub>O–NH<sub>3</sub> mixtures either have weak IR features or ones that overlap severely with spectral bands of H<sub>2</sub>O and NH<sub>3</sub>. For example, hydroxylamine (NH<sub>2</sub>OH) might be expected to form in irradiated H<sub>2</sub>O–NH<sub>3</sub> mixtures, but none of its IR bands are sufficiently well-placed to observe in our spectra (Huston et al., 1983).

Our work with H<sub>2</sub>O–NH<sub>3</sub> ices agrees with results from a recent paper by Loeffler et al. (2006b) who studied 2:1 H<sub>2</sub>O–NH<sub>3</sub> mixtures after irradiation at 70 K. Their spectra show a very weak H<sub>2</sub> feature, and release of both H<sub>2</sub> and N<sub>2</sub> on warming the irradiated sample (detected mass spectrometrically). Also present, but unidentified, in their spectra is a band for NH<sub>4</sub><sup>+</sup> near 1500 cm<sup>-1</sup>, the same as we show in Fig. 13.

In addition to product formation, our radiation experiments showed destruction of the starting materials. The results summarized in Fig. 11 demonstrate that the rate of radiation-induced destruction of NH<sub>3</sub> depends on the initial H<sub>2</sub>O/NH<sub>3</sub> ratio. In pure NH<sub>3</sub>, one fate of radiation products is to reform the starting molecule. In H<sub>2</sub>O–NH<sub>3</sub> mixtures, the presence of H<sub>2</sub>O interferes with such reactions, raising the observed rate of NH<sub>3</sub> destruction. Adding to this effect are the radiation products of H<sub>2</sub>O, such as ions and free radicals, which will combine with both the original NH<sub>3</sub> and its decomposition products, again blocking NH<sub>3</sub> reformation. As but one example of likely reactions, proton transfer from either H<sub>2</sub>O<sup>+</sup> or H<sub>3</sub>O<sup>+</sup> (reaction (2) above) will aid in converting NH<sub>3</sub> into NH<sub>4</sub><sup>+</sup>:

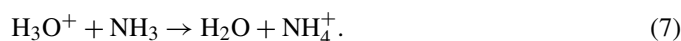
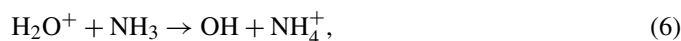


Fig. 11 also hints at a slight temperature dependence for the rate at which H<sub>2</sub>O aids in NH<sub>3</sub> destruction, but the effect appears to be a weak one. Previous experiments on other molecular ices also have shown a dependence of destruction rates on H<sub>2</sub>O content (Hudson et al., 2005) and a weak dependence on temperature (Hudson and Moore, 2004).

Fig. 12 is a quantitative comparison between NH<sub>3</sub> destruction in our radiation experiments and that seen using a different high-energy incident ion (Strazzulla and Palumbo, 1998). The similarity between the data sets reflects the fact that the initial radiation only indirectly influences the subsequent chemistry. It is expected that bombarding ions of somewhat higher stopping power might be more destructive in ices containing H<sub>2</sub>O and NH<sub>3</sub>.

Our experiments showed that radiation-induced reaction chemistry was accompanied by amorphization of crystalline samples, with the rate being largest at the lowest temperatures. This follows a pattern that we, and others, have previously observed (Hudson and Moore, 1995). There are probably multiple reasons for this temperature dependence, one being the greater trapping of product molecules (e.g., H<sub>2</sub>, N<sub>2</sub>) at the lower temperatures. Also, at the higher temperatures, recombination reactions of radiation products should be enhanced, making the crystalline ice appear to be more resistant to amorphization.

## 5. Relevance for icy surfaces

Within the Solar System, radiation-chemical loss of NH<sub>3</sub> occurs in the top most layers of icy surfaces. At the lowest temperature we studied, 10 K, these losses were doubled after ~10 eV molecule<sup>-1</sup> for NH<sub>3</sub> in the presence of H<sub>2</sub>O-ice. We found that H<sub>2</sub>O ices with initial compositions of about 5% NH<sub>3</sub> lost nearly 40% of that substance after ~10 eV molecule<sup>-1</sup> (Charon's dose in about 10<sup>9</sup> years), and we expect the NH<sub>3</sub> signature to be undetectable after 100 eV molecule<sup>-1</sup> (a dose estimated for 10<sup>4</sup> years at Enceladus). This destruction rate is much larger than that for pure NH<sub>3</sub>, and it is driven by the oxidative, and other, chemistry of irradiated H<sub>2</sub>O-ice. On the other hand, for similar radiation doses NH<sub>3</sub> in H<sub>2</sub>O-ice, relevant to Charon, has a lower destruction rate than CH<sub>4</sub> in N<sub>2</sub>-ice, relevant to some terrains on Pluto. In an earlier paper we reported that about 50% of the CH<sub>4</sub> in an N<sub>2</sub> + CH<sub>4</sub> (100:1) ice mixture is destroyed at 10 K for 3 eV molecule<sup>-1</sup>, Pluto's dose in about 3 × 10<sup>8</sup> years (Moore and Hudson, 2003). Therefore, the radiation destruction of NH<sub>3</sub> is not uniquely large.

In addition to radiation chemical losses, sputtering processes (efficient for heavy ions) occur on Solar-System surfaces and could be the dominant mechanism determining the nature of optically-sensed surface ices in some environments. For that reason, whether electrons or O<sup>+</sup> ions, for example, dominate a particular ion flux will determine if sputtering or chemical modification controls the observed chemistry. Future theoretical models need to include the ion-flux composition in the vicinity of objects investigated, along with estimates of the frequency of geologic and exogenic processes that can bring fresh material to a surface.

Our laboratory spectra can be compared among themselves as well as with observational results. In Fig. 14 we have inverted the vertical scale of our spectra to overlay several of them atop Charon data from Cook et al. (2006, 2007). The spectrum of a laboratory H<sub>2</sub>O–NH<sub>3</sub> ice, containing 36 mass % NH<sub>3</sub> and made at ~90 K, is plotted in Fig. 14, and represents a typical amorphous-ice mixture from our work. The exact band positions of the 2.0- and 2.2-μm absorptions change with NH<sub>3</sub> concentration, and the shaded boxes under the peaks indicate the observed ranges. Also, Fig. 14 includes our 2NH<sub>3</sub>·H<sub>2</sub>O and NH<sub>3</sub>·H<sub>2</sub>O spectra, along with arrows to indicate the reported peak positions of NH<sub>3</sub>·2H<sub>2</sub>O (Bertie and Shehata, 1984), and NH<sub>4</sub><sup>+</sup> data from Moore et al. (2003).

The laboratory results in Fig. 14 are compared to the observed spectrum of Charon's anti-Pluto hemisphere (Cook et al., 2006, 2007). Charon's NH<sub>3</sub> minimum was located at 2.2131 μm using fits that had a 13.4% NH<sub>3</sub>·2H<sub>2</sub>O component (Cook et al., 2007). It can be seen from Fig. 14 that amorphous H<sub>2</sub>O–NH<sub>3</sub> mixtures have bands in exactly the same region as the hydrates, so that a unique assignment of the 2.2131-μm feature to a specific crystalline hydrate structure is difficult. Although the quenching of preferred eutectic mixes of NH<sub>3</sub> and H<sub>2</sub>O from Charon cryovolcanism may result in a unique ice stoichiometry, an exclusive spectral identification of hydrates will require more detailed IR information. An equally valid identification for Charon is an amorphous mixture of NH<sub>3</sub> in H<sub>2</sub>O-ice,

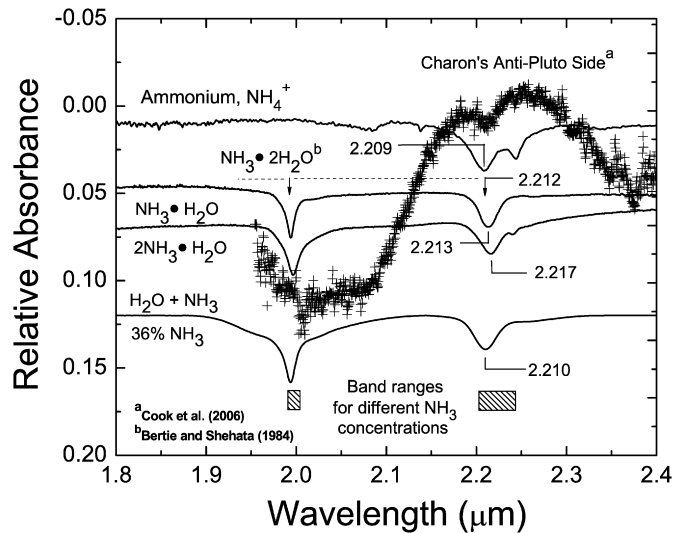


Fig. 14. Laboratory IR spectra of  $2\text{NH}_3\cdot\text{H}_2\text{O}$ ,  $\text{NH}_3\cdot\text{H}_2\text{O}$ , and a mixture deposited at  $\sim 90$  K are compared to the spectrum of Charon's anti-Pluto hemisphere ( $T \sim 42$  K) (Cook et al., 2007). Band positions reported for  $\text{NH}_3\cdot 2\text{H}_2\text{O}$  are also indicated. The ammonium ion's spectrum was measured at 9 K for  $\text{NH}_4\text{Cl}$  (Moore and Hudson, 2003). Spectra are stacked for clarity and scaled to show similar intensities for the  $2.21$   $\mu\text{m}$   $\text{NH}_3$  band.

again as seen in Fig. 14. The comparisons between laboratory data and observed spectra in Fig. 14 are illustrative. A correct comparison is possible only by using models (Hapke, Shkuratov, etc.) and the knowledge of the optical constants of the model species.

These points are further illustrated in Fig. 15 which summarizes the near-IR band positions of  $2\text{NH}_3\cdot\text{H}_2\text{O}$ ,  $\text{NH}_3\cdot\text{H}_2\text{O}$ , and the amorphous  $\text{H}_2\text{O}\text{--}\text{NH}_3$  ices of Fig. 8. The two trapezoidal figures enclose the set of positions that resulted from variations of temperature and amorphous-ice composition. Fig. 15 shows that above 90 K the hydrates' IR band positions are very close to one another. Further, the figure suggests that hydrate band positions will be indistinguishable from those of amorphous  $\text{H}_2\text{O}\text{--}\text{NH}_3$  ice mixtures of similar composition. Such is certainly the case for  $2\text{NH}_3\cdot\text{H}_2\text{O}$ , the hydrate for which we have the most data.

We showed that both the 2.2- and 2.0- $\mu\text{m}$   $\text{NH}_3$  bands are detectable in laboratory spectra, even for mixtures as dilute as 1.6%  $\text{NH}_3$ . However, to date the 2.0- $\mu\text{m}$   $\text{NH}_3$  band has not been reported on any icy surface. This non-detection may be related to spectral modeling that factors in scattering and grain size. Fig. 14 shows that another nitrogen species, the ammonium ion, has only one prominent band in the 1.8–2.4  $\mu\text{m}$  region, at 2.2  $\mu\text{m}$ . Ammonia, a base, can react with acids even at temperatures as low as 155 K, near the crystallization temperature for amorphous  $\text{H}_2\text{O}$ -ice, to form  $\text{NH}_4^+$  (Moore and Hudson, 2003). Also, we have reported in this paper that  $\text{NH}_4^+$  forms in irradiated  $\text{H}_2\text{O} + \text{NH}_3$  ices. Thus it is chemically reasonable to consider that  $\text{NH}_4^+$  is present in Solar System ices, and may contribute to the 2.21- $\mu\text{m}$  feature seen on Charon and elsewhere. Once formed,  $\text{NH}_4^+$  is expected to be thermally stable.

Changes in the 2.21- $\mu\text{m}$  band's position in icy mixtures terminate at  $4527$   $\text{cm}^{-1}$  ( $2.209$   $\mu\text{m}$ ) for ices with  $\sim 1.6\%$   $\text{NH}_3$ .

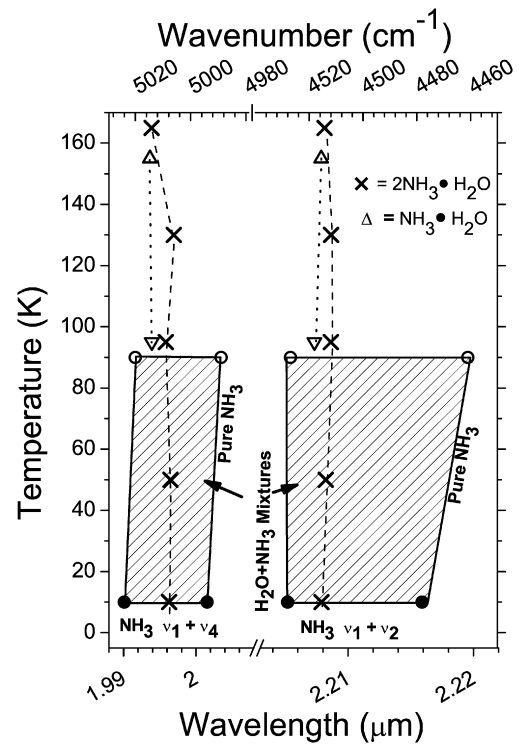


Fig. 15. The wavelength range covered by the  $\text{NH}_3$  ( $\nu_1 + \nu_2$ ) and ( $\nu_1 + \nu_4$ ) bands in  $\text{H}_2\text{O}\text{--}\text{NH}_3$  ices at 10 and 90 K coincides with the range of the near-IR bands of  $2\text{NH}_3\cdot\text{H}_2\text{O}$  and  $\text{NH}_3\cdot\text{H}_2\text{O}$  at different temperatures.

Further shifts were not observed with either temperature or radiation exposure. Therefore, it is difficult to use a single nitrogen-containing species to explain the bands seen on both the anti-Pluto side of Charon at  $2.2131$   $\mu\text{m}$  ( $4525$   $\text{cm}^{-1}$ ) and the sub-Pluto side at  $2.1995$   $\mu\text{m}$  ( $4546$   $\text{cm}^{-1}$ ) (Cook et al., 2007). It is likely that further laboratory experiments will be needed to solve this problem. Shifts in the  $\text{NH}_4^+$  band positions for different ice compositions, and thermal and radiation histories, along with possible shifts in the  $\text{NH}_3$  bands with different matrices, need to be examined.

### Acknowledgments

The authors thank Jason Cook and Dr. Steven Desch at Arizona State University for providing observational data on Charon for comparison with our laboratory results, for providing a preprint of their upcoming paper on Charon, and for several helpful conversations. The authors are very grateful to Drs. J.E. Bertie and M.M. Morrison who provided original data files for the hemihydrate and monohydrate. We acknowledge Dr. Perry Gerakines who worked on the acid/ $\text{NH}_3$  experiments while an NRC postdoc in our laboratory. The authors acknowledge support through NASA's Planetary Atmospheres and Planetary Geology and Geophysics programs, as well as support from the NASA Astrobiology Institute's Goddard Center for Astrobiology. In addition, we thank Steve Brown, Claude Smith, and Eugene Gerashchenko, members of the Radiation Laboratory at NASA Goddard, for operation of the Van de Graaff accelerator. R.L.H. acknowledges separate support from

NASA Grant NAG-5-1843. R.F.F. and J.N.S. gratefully acknowledge the Office of Naval Research for partial support of this work on funding Document N0001404WR20147.

## References

- Baratta, G.A., Leto, G., Spinella, F., Strazzulla, G., Foti, G., 1991. The 3.1  $\mu\text{m}$  feature in ion-irradiated water ice. *Astron. Astrophys.* 252, 421–424.
- Bauer, J.M., Roush, R.L., Geballe, T.R., Meech, K.J., Owen, T.C., Vacca, W.D., Rayner, J.T., Jim, K.T.C., 2002. The near-infrared spectrum of Miranda. *Icarus* 158, 178–190.
- Bertie, J.E., Devlin, J.P., 1984. The infrared spectra and phase transitions of pure and isotopically impure  $2\text{ND}_3 \cdot \text{H}_2\text{O}$ ,  $2\text{NH}_3 \cdot \text{D}_2\text{O}$ ,  $2\text{NH}_3 \cdot \text{H}_2\text{O}$ , and  $2\text{ND}_3 \cdot \text{D}_2\text{O}$  between 100 and 15 K. *J. Chem. Phys.* 81, 1559–1572.
- Bertie, J.E., Morrison, M.M., 1980. The infrared spectra of the hydrates of ammonia,  $\text{NH}_3 \cdot \text{H}_2\text{O}$  and  $2\text{NH}_3 \cdot \text{H}_2\text{O}$  at 95 K. *J. Chem. Phys.* 73, 4832–4837.
- Bertie, J.E., Shehata, M.R., 1984. Ammonia dihydrate: Preparation, X-ray powder diffraction pattern and infrared spectrum of  $\text{NH}_3 \cdot 2\text{H}_2\text{O}$  at 100 K. *J. Chem. Phys.* 81, 27–30.
- Bertie, J.E., Shehata, M.R., 1985. The infrared spectra of  $\text{NH}_3 \cdot \text{H}_2\text{O}$  and  $\text{ND}_3 \cdot \text{D}_2\text{O}$  at 100 K. *J. Chem. Phys.* 83, 1449–1456.
- Brown, W.L., Lanzerotti, L.J., Johnson, R.E., 1982. Fast ion bombardment of ices and its astrophysical implications. *Science* 218, 525–531.
- Brown, M.E., Calvin, W.M., 2000. Evidence for crystalline water and ammonia ices on Pluto's satellite Charon. *Science* 287, 107–109.
- Cook, J.C., Desch, S.J., Roush, T., Geballe, T.R., Trujillo, C.A., 2006. Near-infrared spectra of Charon: Support for cryovolcanism on Kuiper belt objects? *Lunar Planet. Sci. XXXVII*. Abstract 2107.
- Cook, J.C., Desch, S.J., Roush, T., Trujillo, C.A., Geballe, T.R. 2007. Near-infrared spectroscopy of Charon: Possible evidence for cryovolcanism on Kuiper belt objects. *Astrophys. J.*, in press.
- Cooper, J.F., Christian, E.R., Richardson, J.D., Wang, C., 2003. Proton irradiation of Centaur, Kuiper belt, and Oort cloud objects at plasma to cosmic ray energy. *Earth Moon Planets* 92, 261–277.
- Dumas, C., Terrile, R.J., Brown, R.H., Schneider, G., Smith, B.A., 2001. Hubble space telescope NICMOS spectroscopy of Charon's leading and trailing hemispheres. *Astron. J.* 121, 1163–1170.
- Emery, J.P., Burr, D.M., Cruikshank, D.P., Brown, R.H., Dalton, J.B., 2005. Near-infrared (0.8–4.0  $\mu\text{m}$ ) spectroscopy of Mimas, Enceladus, Tethys, and Rhea. *Astron. Astrophys.* 435, 353–362.
- Gerakines, P.A., Bray, J.J., Davis, A., Richey, C.R., 2005. The strengths of near-infrared absorption features relevant to interstellar and planetary ices. *Astrophys. J.* 620, 1140–1150.
- d'Hendecourt, L.B., Allamandola, L.J., 1986. Time dependent chemistry in dense molecular clouds. III. Infrared band cross sections of molecules in the solid state at 10 K. *Astron. Astrophys. Suppl. Ser.* 64, 453–467.
- Hudgins, D.M., Sandford, S.A., Allamandola, L.J., Tielens, A.G.G.M., 1993. Mid- and far-infrared spectroscopy of ices: Optical constants and integrated absorbances. *Astrophys. J. Suppl. Ser.* 86, 713–870.
- Hudson, R.L., Moore, M.H., 1995. Far-IR spectral changes accompanying proton irradiation of solids of astrochemical interest. *Radiat. Phys. Chem.* 45, 779–789.
- Hudson, R.L., Moore, M.H., 2004. Reactions of nitriles in ices relevant to Titan, comets, and the interstellar medium: Formation of cyanate ion, ketenimines, and isonitriles. *Icarus* 172, 466–478.
- Hudson, R.L., Moore, M.H., 2006. Infrared spectra and radiation stability of  $\text{H}_2\text{O}_2$  ices relevant to Europa. *Astrobiology* 6, 483–489.
- Hudson, R.L., Moore, M.H., Gerakines, P.A., 2001. Radiation chemical alterations in Solar System ices: An overview. *J. Geophys. Res. Planets* 106, 33275–33284.
- Hudson, R.L., Moore, M.H., Cook, A.M., 2005. IR characterization and radiation chemistry of glycolaldehyde and ethylene glycol ices. *Adv. Space Res.* 36, 184–189.
- Huston, T., Hisatsune, I.C., Heicklen, J., 1983. Low-temperature infrared studies of some acid–base reactions. *Can. J. Chem.* 61, 2077–2088.
- Jewitt, D.C., Luu, J., 2004. Crystalline water ice on the Kuiper belt object (50000) Quaoar. *Nature* 432, 731–733.
- Johnson, R.E., Lanzerotti, L.J., Brown, W.L., Augustyniak, W.M., Mussil, E., 1983. Charged particle erosion of frozen volatiles in ice grains and comets. *Astron. Astrophys.* 123, 343–346.
- Kargel, J.S., 1992. Ammonia–water volcanism on icy satellites: Phase relations at 1 atmosphere. *Icarus* 100, 556–574.
- Krimigis, S.M., Armstrong, T.P., Axford, W.I., Cheng, A.F., Gloeckler, G., Hamilton, D.C., Keath, E.P., Lanzerotti, L.J., Mauk, B.H., 1986. The magnetosphere of Uranus: Hot plasma and radiation environment. *Science* 233, 97–102.
- Leliwa-Kopystyński, J., 2002. The water–ammonia phase diagram up to 300 MPa: Application to icy satellites. *Icarus* 159, 518–528.
- Lewis, J.S., 1972. Low temperature condensation from the solar nebula. *Icarus* 16, 241–252.
- Loeffler, M.J., Raut, U., Vidal, R.A., Baragiola, R.A., Carlson, R.W., 2006a. Synthesis of hydrogen peroxide in water ice by ion irradiation. *Icarus* 180, 265–273.
- Loeffler, M.J., Raut, U., Baragiola, R.A., 2006b. Enceladus: A source of nitrogen and an explanation for the water vapor plume observed by Cassini. *Astrophys. J.* 649, L133–L136.
- Mastrapa, R.M.E., Brown, R.H., 2006. Ion irradiation of crystalline  $\text{H}_2\text{O}$  ice: Effect on the 1.65- $\mu\text{m}$  band. *Icarus* 183, 207–214.
- Moore, M.H., Hudson, R.L., 1992. Far-infrared spectral studies of phase changes in water ice induced by proton irradiation. *Astrophys. J.* 401, 353–360.
- Moore, M.H., Hudson, R.L., 1994. Far-infrared spectra of cosmic-type pure and mixed ices. *Astron. Astrophys. Suppl. Ser.* 103, 45–56.
- Moore, M.H., Hudson, R.L., 1998. Infrared study of ion irradiated water ice mixtures with organics relevant to comets. *Icarus* 135, 518–527.
- Moore, M.H., Hudson, R.L., 2000. IR detection of  $\text{H}_2\text{O}_2$  at 80 K in ion-irradiated laboratory ices relevant to Europa. *Icarus* 145, 282–288.
- Moore, M.H., Hudson, R.L., 2003. Infrared study of ion-irradiated  $\text{N}_2$ -dominated ices relevant to Triton and Pluto: Formation of HCN and HNC. *Icarus* 161, 486–500.
- Moore, M.H., Donn, B., Khanna, R., A'Hearn, M.F., 1983. Studies of proton irradiated cometary-type ice mixtures. *Icarus* 54, 388–405.
- Moore, M.H., Hudson, R.L., Ferrante, R.F., 2003. Radiation products in processed ices relevant to Edgeworth–Kuiper belt objects. *Earth Moon Planets* 92, 291–306.
- Sill, G., Fink, U., Ferraro, J.R., 1981. The infrared spectrum of ammonia hydrate: Explanation for a reported ammonia phase. *J. Chem. Phys.* 74, 997–1000.
- Sittler Jr., E.C., Johnson, R.E., Smith, H.T., Richardson, J.D., Jurac, S., Moore, M., Cooper, J.F., Mauk, B.H., Michael, M., Paranicas, C., Armstrong, T.P., Tsurutani, B., 2006. Energetic nitrogen ions within the inner magnetosphere of Saturn. *J. Geophys. Res.* 111, A09223.
- Spinks, J.W.T., Woods, R.J., 1990. *An Introduction to Radiation Chemistry*, third ed. Wiley, New York.
- Strazzulla, G., Palumbo, M.E., 1998. Evolution of icy surfaces: An experimental approach. *Planet. Space Sci.* 46, 1339–1348.
- Strazzulla, G., Leto, G., Baratta, G.A., Spinella, F., 1991. Ion irradiation experiments relevant to cometary physics. *J. Geophys. Res.* 96, 17547–17552.
- Strazzulla, G., Cooper, J.F., Christian, E.R., Johnson, R.E., 2003. Ion irradiation of TNOs: From the fluxes measured in space to the laboratory experiments. *C. R. Phys.* 4, 791–801.
- Swallow, A.J., 1973. *Radiation Chemistry*. Wiley, New York.
- Theophanides, T., Turrell, G.C., 1967. Infrared study of thermal decomposition of the azide ion. *Spectrochim. Acta* 23, 1927–1935.
- Verbiscer, A.J., Peterson, D.E., Skrutskie, M.F., Cushing, M., Helfenstein, P., Nelson, M.J., Smith, J.D., Wilson, J.C., 2006. Near-infrared spectra of the leading and trailing hemispheres of Enceladus. *Icarus* 182, 211–223.
- Ziegler, J.P., Biersack, J.P., Littmark, U., 1985. *The stopping and range of ions in solids*. Pergamon, New York. See also <http://www.srim.org>.